ELSEVIER

Coordination Chemistry Reviews 228 (2002) 343–363

COORDINATION CHEMISTRY REVIEWS

www.elsevier.com/locate/ccr

Review of binding methods and detection of Al(III) binding events in trypsin and DL-DPPC liposomes by a general thermodynamic model

Vito Di Noto [a,*], Lisa Dalla Via [b], Paolo Zatta [c]

[a] *Dipartimento di Chimica Inorganica, Metallorganica ed Analitica, Università di Padova, Via Loredan 4, I-35131 Padova, Italy*
[b] *Dipartimento di Scienze Farmaceutiche, Università di Padova, Via Marzolo 5, I-35131 Padova, Italy*
[c] *Dipartimento di Biologia, Centro CNR Metalloproteine, Università di Padova, Via G. Colombo 3, I-35131 Padova, Italy*

Received 14 August 2001; accepted 15 March 2002

Contents

Abstract

In this paper are reviewed some of the most useful binding formalisms which have been developed in order to investigate the diversity of the commonly encountered receptor–ligand systems. Particularly, our attention is focused on the presentation and application of a general and rigorous thermodynamic treatment which explains in a simple and coherent way the non-linear profiles observed in the experimental binding, Scatchard, Hill and Adair plots. By applying this model, both qualitative and detailed quantitative investigations were carried out on the binding process of Al(III) to trypsin and DL-dipalmitoylphosphatidylcholine

* Corresponding author. Fax: +390-049-8275161.
E-mail address: vito.dinoto@unipd.it (V. Di Noto).

PII: S0010-8545(02)00083-8

(DPPC) liposomes. Particularly, it has been demonstrated that: Al(III) interacts with liposomes in two binding sites with very different dissociation constants. The first one has been calculated to be 0.0168 μmol l^{-1} and the second 2.833 μmol l^{-1}. The first is referred to the preferential interaction of Al^{3+} with the polar head of the phospholipid, while the second most likely regards the interaction of Al^{3+} with other peripheral sites. On the other hand, Al^{3+} interacts with trypsin in two types of binding sites. The first binding site with $K_{1,1} = 0.2531$ μmol l^{-1} and the second with $K_{2,1} = 1.424$ μmol l^{-1}.

Keywords: Binding site; Ligand–receptor interactions; Aluminium; Trypsin; Liposomes

1. Introduction

The study of the binding processes constitutes a crucial step for the comprehension of the molecular mechanisms which account for many biological events. Investigation on the mode of binding of many synthetic molecules to biological macromolecules, such as DNA, is the starting point for the synthesis of new drugs. Otherwise, the study of the binding to cellular targets for many natural or synthetic compounds, ions or molecules, permits one to understand the molecular mechanism accountable for the pathologic effects of many diseases.

The term binding indicates the interaction between a substrate S, and a ligand L, whose concentration constitutes the independent variable of the system [1]. The types of interactions characterising the binding processes can be so grouped: *electrostatic* [2], *induction* (*or polarisation*) *forces and dispersion* (*or van der Waals*) *forces.* The non-covalent interactions play a crucial role in the structure and regulation of the living systems. Certainly, the O_2–haemoglobin system [3,4] represents one of the more classic examples of molecular association. Besides this example, a series of receptors such as the porphyrin or ferredoxins are involved in the binding of small molecules (O_2, CO, CO_2 and N_2) [5]. Moreover, study of the binding between an enzyme and its substrate is of fundamental importance to understand the mechanisms that regulate the living being. The metabolic events include the more known examples of these interactions, but also the neurotransmission (i.e. the interaction between the neurotransmitter and the synaptic receptors [6,7]) and the genetic expression (i.e. the interaction between proteins and nucleic acids [8–10]) depend on these types of phenomena. Studies in this field are devoted also on more empirical sectors such as the use of immobilised enzymes or the biomimetic catalysis for the development and the production of drugs. Moreover, study of the interactions which take place between nucleic acids and a wide range of ligands is important: the relevance of these binding processes lies with the possibility either to obtain the molecular information required for the synthesis of new efficient antitumor drugs [11,12] or to understand the biological mechanisms which involve nucleic acids. Further general pharmacological applications where the investigations of the binding phenomena are fundamental concerns in the field of supramolecular chemistry [13–16], where innovative receptors or transport systems for drugs and metallic ions are investigated. These types of binding complexes have also found interesting application as linking phases in LC and HPLC chromatographic analysis [17,18].

The study of the binding plays also a key role in the field of industrial catalysis where the preparation of efficient catalysts requires the development of methods to determine the thermodynamic and kinetic binding parameters of the system considered.

Moreover, the investigation of molecular association processes are important in the determination of the adsorption mechanisms of small molecules [19] or ions [20] (environmental applications etc.) and in the chemistry of functional materials (semiconductors [21], sensors [21,22], etc.).

As the binding phenomena are involved in a wide range of processes and applications, it is necessary to develop accurate and general methods which permit us to characterise fully the systems under analysis.

In this paper the widely used binding models will be reviewed and briefly discussed. Moreover, a recent thermodynamic model [23], developed in our laboratory, will be described in order to underline its capacity and properties with respect to the previous ones. Finally, the application of the model mentioned above to the study of the binding of the Al(III) to trypsin and DL-dipalmitoylphosphatidylcholine (DPPC) liposomes will be reported.

Al(III) is a well-known toxic agent and represents a severe problem for a variety of medical as well as environmental situations [24]. While the role of Al(III) as a causative agent of dialysis dementia is now well-established [25] its involvement as a potential etiopathogenic factor in several neurodegenerative diseases included Alzheimer's disease (AD) is still matter of debate and intense investigation. Much attention has been paid to the protease and protease inhibitors dismetabolism in relation to the amyloid formation in AD [26,27]. Several reports in this connection suggested that proteases and their inhibitors might have a relevant etiopathogenic role in AD [28] as well as in other neurodegenerative diseases with amyloid deposition [13]. In a previous study we demonstrated that Al(III) can be a candidate

for playing a dismetabolic role in inhibiting the proteolytic activity of the serine protease enzyme like trypsin and α-chymotrypsin [29]. In addition, the interaction between Al(III) and trypsin has been carried out in these laboratories studying the conformation of trypsin–Al(III) complex in solution by Raman and Fourier transform infrared attenuated total reflectance spectroscopy [30]. The results indicated that Al(III) influences the secondary structure of trypsin. In particular the interaction between trypsin and Al(III) in solution determines a decrease in the percentage of the α-helix and an increase of β-sheet and random coil conformational status.

Several models have been proposed to study the molecular mechanisms that could justify Al(III) toxicity [31,32]. In order to understand the characteristics of the interaction between Al(III) and cell membrane, a liposomes model has been used. Liposomes were utilized extensively by our laboratories to better understand the interaction between phospholipids and Al(III) [33]. While, as a general model for the study of the interaction between Al(III) and a protein, trypsin was chosen as described in this paper. Thus, both these models were paradigmatically used as an applicative aspect of the thermodynamic model here exhaustively described [23,34].

2. Binding models

The main goal of the receptor–ligand investigations is the determination of the binding constants or affinity constants at equilibrium [1].

If we consider a solution containing both the ligand L and the substrate S, the property y that depends on the total ligand concentration (L_t) has to be measured. The system is described by Ref. [1]:

$$y_i = f([L]_i,\ \mu_i) \tag{1a}$$

$$L_{ti} = g([L]_i,\ \lambda_k) \tag{1b}$$

In these equations y_i, which is the dependent variable, is the value of the measured property at total ligand concentration L_{ti}; $[L]_i$ is the free ligand concentration corresponding to L_{ti}; μ_i and λ_k are parameters. Eq. (1a) is named as a generalised isotherm or binding isotherm [1].

The explicit form of the isotherms and the nature of the parameters depend on the system being studied and on the assumed stoichiometric model. For this reason to obtain useful functions, it was necessary to develop a series of models that will be described briefly below.

In general, the following classification can be done [1,35,36]:

1) *Independent site models*: These models presuppose no or negligible interactions between the ligand molecules complexed with the receptor. This latter can have only one type of site or multiple classes of independent sites.
2) *Non-independent site models*: These models can be grouped into two categories: *allosteric:* the binding toward a particular site modify the affinity of the substrate with respect to the other ligand units. In this case two different interactions with positive cooperativity and anticooperativity can be recognised. In the first case the finding of the subsequent ligand is promoted, whereas secondly, an inhibitory effect takes place; *sequential:* in these models the interactions between ligand molecules which are located in contiguous sites play the most important role.

In the following paper the interactions of receptor–ligand for systems with only one type of ligand are described and the effects of the solvent are neglected.

2.1. Characteristic parameters of the binding systems. Graphic presentation

For the sake of clarity it is useful to introduce the definition of some physical parameters which are usually employed to in the binding models.

The fractional saturation Y_i of site ith [1,35]:

$$Y_i = \frac{[\text{Bound site } i]}{[\text{Free site } i] + [\text{Bound site } i]}. \tag{1}$$

The summation of the fractional saturation for all the n sites gives us the number of moles of ligand bound per mole of substrate, B:

$$B = \frac{\sum_{i=0}^{n} i[SL_i]}{\sum_{i=0}^{n}[S_i]} \tag{2}$$

where SL_i represents the total amount of microscopic species of type i (S_i) which contain bound species L and n is the total number of sites in the substrate. Generally, in the binding evaluations, B constitutes the dependent variable: the graphic representation of B versus the concentration of free ligand [L] is named the *direct binding plot* [1], Fig. 1. The curve shape of this plot, for non-cooperative phenomena, resembles that of one-half of one branch of a rectangular hyperbola and shows the behaviour of the saturation of the substrate increasing [L], whilst, it exhibits a sigmoidal form if interactions between ligands occur [1,37]. When more than one type of site is present, the resultant graph is the summation of the curves relative to each type of site. Thus, it is possible to obtain a characteristic B versus [L] curve where 'steps' are detected (see Fig. 1).

This method of graphic representation has a disadvantage: it becomes remarkably inaccurate for high values of B and [L]. For these reasons other kinds

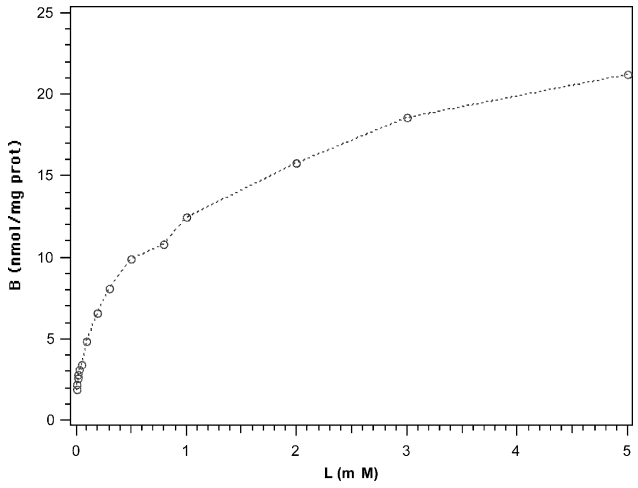

Fig. 1. Hypothetical binding plot. [B] is the concentration of ligand bound to the receptor and [L] is the free ligand concentration.

of plots are preferred. Among these, the most common is the so called *Scatchard plot* [38,39] where the ratio B/[L] is plotted versus B. The Scatchard representation is considered one of the most suitable to describe binding systems because it is able to provide the parameters describing the isotherm in a simple manner. Moreover, Scatchard curves show remarkable variability in their profiles in dependence on the characteristics of the system under investigation. For these reasons, this representation allows us to carry out accurate fitting in order to evaluate the binding parameters.

McGhee and von Hippel [40] compared the Scatchard plot with respect to the following representations: $1/B$ versus 1/[L] and [L]/B versus [L], concluding that the last two types are less efficient to point out non-linear behaviour.

The different shapes of the curves and their meaning will be discussed briefly later [1,35,41–43].

Noteworthy, cooperative phenomena are commonly studied by using the *Hill plot* [44] or log–log plot. In this representation $\ln(Y/1-Y))$ is plotted versus ln[L]. The slope of these curves yield the Hill constant, n_H, whose meaning will be elucidated below.

2.2. Binding constants

To make clear the meaning of the binding constants it is useful to define briefly the differences between macroscopic and microscopic constants [1,35]. This appears to be particularly important when equilibria which involve multiple classes of sites are considered.

Assuming as model example the dibasic species H_2A^{2+} we can write the following macroscopic equilibria:

$$H_2A^{2+} \leftrightarrow HA^+ + H^+$$

$$HA^+ \leftrightarrow A + H^+$$

and the corresponding macroscopic dissociation constants:

$$K_1 = \frac{[HA^+][H^+]}{[H_2A^{2+}]} \quad (3)$$

$$K_2 = \frac{[A][H^+]}{[HA^+]}. \quad (4)$$

In this case the microscopic states are represented by:

a) H_2A^{2+};
b) HA^+, AH^+;
c) A.

These microscopic states are involved in microscopic equilibria which are characterized by the corresponding dissociation constants:

$$H_2A^{2+} \leftrightarrow HA^+ + H^+ \quad k_1;$$

$$H_2A^{2+} \leftrightarrow AH^+ + H^+ \quad k_2;$$

$$HA^+ \leftrightarrow A + H^+ \quad k_3;$$

$$AH^+ \leftrightarrow A + H^+ \quad k_4.$$

On this basis, it is easy to conclude that microscopic and macroscopic constants are linked together by the following relationships [35]:

$$K_1 = k_1 + k_2 \quad (5)$$

and

$$\frac{1}{K_2} = \frac{1}{k_3} + \frac{1}{k_4}. \quad (6)$$

Furthermore, the four microscopic constants are not independent:

$$k_1k_3 = k_2k_4 = K_1K_2. \quad (7)$$

To the reader, this simple description is a concrete example of the meaning of microscopic and macroscopic constants and of their interrelationships. As second example, we consider a situation where statistical effects are important. Let us assume that the two sites of the H_2A^{2+} specie are identical and independent (for example a long-chain aliphatic diamine). In this case, all the microscopic equilibrium constants have the same value.The macroscopic equilibria are:

$$A + H^+ \leftrightarrow A(H^+)_1$$

$$A(H^+)_1 + H^+ \leftrightarrow A(H^+)_2$$

and the corresponding dissociation constants are given by:

$$K_1 = \frac{([A][H^+])}{[A(H^+)_1]} \quad (8)$$

$$K_2 = \frac{([A(H^+)_1][H^+])}{[A(H^+)_2]} \quad (9)$$

Finally, by taking into account the microscopic equilibria it is possible to conclude that the macroscopic constants are related to the microscopic constants by the following equations:

$$K_1 = k/2; \quad K_2 = 2k. \quad (10)$$

Thus, in principle, even though the microscopic dissociation constant is the same for each ionisation, the statistical effects make K_1 four times smaller than K_2.

2.3. Binding approaches

2.3.1. Independent site models

In this type of model it is assumed that, inside each class of sites, the microscopic dissociation constant is the same independently from the overall site filling condition of the system.

2.3.1.1. Identical sites. In this description, it is assumed that the receptor S contains n sites for the ligand L and that the value of the microscopic constant is k for each of the following equilibria:

$$S_0 + L \leftrightarrow SL_1$$
$$SL_1 + L \leftrightarrow SL_2$$
$$\vdots$$
$$SL_{n-1} + L \leftrightarrow SL_n$$

The n-th index indicates the overall number of L molecules bound to the system. In general, it is possible to calculate all the different ways by which a number of ith ligands could find to n sites. This quantity is named the statistic factor $\Omega_{n,i}$ and is thus defined [35]:

$$\Omega_{n,i} = \frac{n!}{(n-i)!i!}. \quad (11)$$

In order to obtain an equation of B as a function of the concentration of free ligand [L], the concentrations SL_i, shown in Eq. (2), can be expressed in terms of macroscopic dissociation constants.

The relationship between k and K_i is driven by the statistical factor $\Omega_{n,i}$. Indeed, it can be easily demonstrated that:

$$B = \frac{\sum_{i=1}^{n} i\left[\prod_{j=1}^{i}(n-j+1)/j\right]([L]/k)^i}{1 + \sum_{i=1}^{n}\left[\prod_{j=1}^{i}(n-j+1)/j\right]([L]/k)^i} \quad (12)$$

Taking into account that:

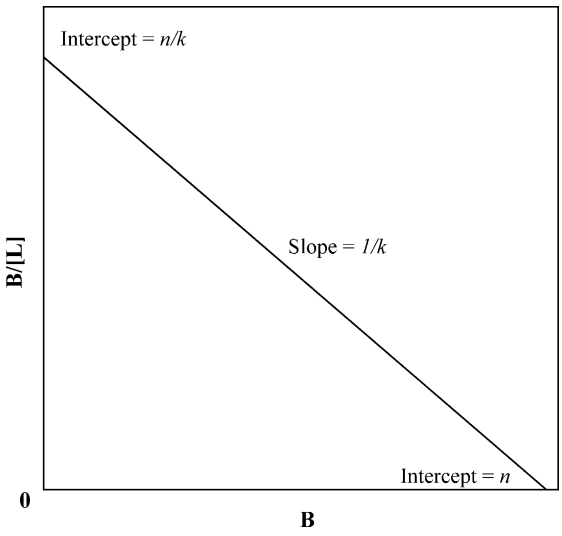

Fig. 2. Scatchard plot for a receptor with identical independent binding sites (adapted from Ref. [35]).

$$\prod_{j=1}^{i}\left(\frac{n-j+1}{j}\right) = \frac{n!}{(n-1)!i!} \quad (13)$$

Eq. (12) becomes [1,35]:

$$B = \frac{n[L]/k}{1 + [L]/k} \quad (14)$$

from which it is easy to obtain the equation of the Scatchard plot:

$$\frac{B}{[L]} = \frac{n}{k} - \frac{B}{k}. \quad (15)$$

Eq. (15) represents a straight line whose slope will be $-1/k$ and the intercepts on ordinate and abscissa axes will be n/k and n, respectively (Fig. 2).

2.3.1.2. Multiple classes of independent sites (Adair model). In this case, it is hypothesised that in the receptor are present N classes of n_i independent sites of ith type characterized by k_i intrinsic microscopic dissociation constant. Particularly, ion–metal coordination [45], binding of small molecules with macromolecules, such as enzymes, nucleic acids, or synthetic polymers [46,47] can be described by this model.

In a similar fashion to the discussion reported above concerning a system containing one class of independent site, the so-called Adair equation [48] can be easily obtained:

$$B = \sum_{i=1}^{N}\left\{\frac{n_i[L]/k_i}{1 + ([L]/k_i)}\right\} \quad (16)$$

from which:

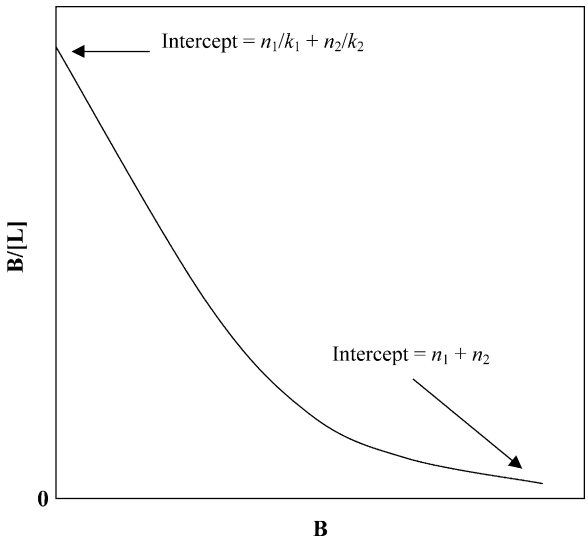

Fig. 3. Typical biphasic Scatchard plot (adapted from Ref. [35]).

$$\frac{B}{[\mathrm{L}]} = \sum_{i=1}^{N} \left\{ \frac{n_i/k_i}{1 + ([\mathrm{L}]/k_i)} \right\} \tag{17}$$

As depicted in Fig. 3, this latter equation describes a non-linear Scatchard profile, characterised by an upward convexity. From analysis of this plot, the intercepts in the ordinate and in the abscissa allows us to determine the values of $\Sigma_i(n_i/k_i)$ and $\Sigma_i(n_i)$, respectively. As occurs in the cases of metal ion coordination the values of n_i can be easily calculated if, at least roughly, the structure of the receptor is known. Nevertheless, this approach becomes more difficult for the macromolecular systems due to the fact that weak statistical considerations or doubtful graphical extrapolations constitute the unique reference data. The Adair equation has been frequently used to treat binding data by graphical methods [1,35], assuming that, between the possible interpolating curves, the best fit is that determined using the lower number of parameters.

Nevertheless, the use of graphical methods present the following problems:

1) the evaluation of the intercepts is error prone, especially with those plots where a high degree of curvature is present;
2) in the absence of structural information, the choice of the number of classes of sites could be an arbitrary procedure;
3) cooperative phenomena could be responsible for the curvature of the plots.

Notwithstanding these uncertainties, graphical methods have been widely used instead of non-linear minimisation analysis owing to the fact that this latter requires a first evaluation of starting parameters and could give rise to unrealistic parameters if a relative local minimum is obtained by the minimisation procedures [43,49–51].

2.3.2. Cooperative or allosteric models

The involvement of cooperative phenomena implies that the coordination of a ligand modifies the affinity of the receptor towards other potential binding ligands, so producing a continuous modulation of the microscopic dissociation constant. These phenomena can be considered as general and realistic because the steric and electrostatic effects associated to the complexation of a ligand could induce conformational changes in the substrate so affecting the reactivity of the free sites toward ligands. Classical examples of these events are encountered in proteinaceous substrates, such as enzymes or transport proteins as haemoglobin etc.

Until now, the cooperative phenomena were investigated by the introduction of semi-empirical arbitrary functions and parameters into thermodynamic quantities describing the physical status of the system.

For the simple case of a class of identical sites, the microscopic dissociation constant for $B = 0$ was assumed k_0. As B increases, the interactions that take place between the sites provoke a modification of k.

The difference of free standard energy for the dissociation of a ligand is [35]:

$$\Delta G^0 = \Delta G_0^0 + RT\ \phi(B) \tag{18}$$

where

$$\Delta G_0^0 = -RT\ \ln(k_0) \tag{19}$$

and $\phi(B)$ is a completely arbitrary function, that, by definition, takes into account the effects of interactions between sites varying with the degree of saturation. The explicit form of $\phi(B)$ can be deduced so as to explain any type of data. Tanford estimated $\phi(B)$ for the association of ions with a charged macromolecule [46] by a simple electrostatic theory.

From Eq. (18) it is possible to obtain:

$$k(B) = k_0\ \mathrm{e}^{-\phi(B)} \tag{20}$$

where $\phi(B)$ is zero at $B = 0$. The expression for $k(B)$ can be introduced in Eq. (14):

$$B = \frac{n[\mathrm{L}]/k(B)}{1 + ([\mathrm{L}]/k(B))} \tag{21}$$

If $\phi(B)$ is a decreasing function of B, then $k(B)$ increases as saturation proceeds, so producing a curved Scatchard plot with an upward convexity. Nevertheless, in this representation an upward convexity is also expected for a receptor with more classes of independent sites. However, this latter situation seems not to be realistic, especially for biological receptors.

Otherwise, when $\phi(B)$ increases as B increases, then the Scatchard plot shows a downward convexity and a

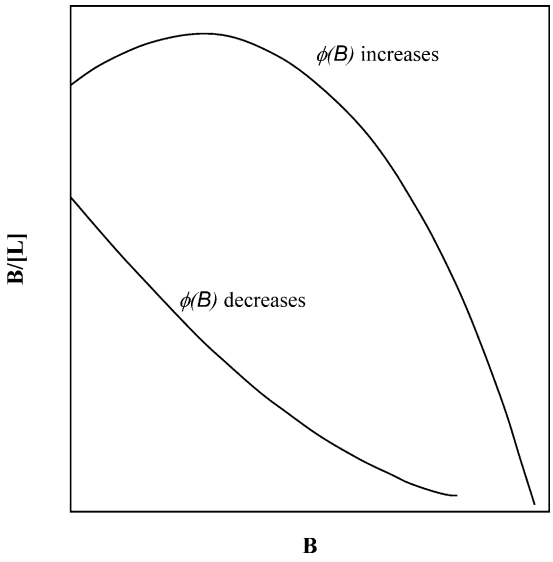

Fig. 4. Hypothetical shapes of Scatchard plots for the cases where $\phi(B)$ decreases or increases with increasing B (adapted from Ref. [35]).

positive cooperativity takes place. The behaviours of the two Scatchard plots are depicted in Fig. 4.

In the general case where there are several classes of interacting sites, then Eq. (20) becomes:

$$k_i(B) = k_{0,i}\, e^{-\phi_i(B)} \tag{22}$$

where $k_{0,i}$ is the intrinsic microscopic dissociation constant at $B=0$ for sites in class i, and $\phi_i(B)$ is the interaction function for sites in class i.

Furthermore, for macroscopic dissociation constants it is necessary to carry out a correction owing to the fact that statistical effects introduce some apparent anticooperativity into the binding equilibria. To correct this, the intrinsic standard free energy change associated with binding of the ith ligand in a series as ΔG_i^0, is defined. This is:

$$\Delta G_i^0 = RT \ln K_i - RT \ln(\Omega_{n,i-1}/\Omega_{n,i}) \tag{23}$$

The K_i represents the dissociation macroscopic constants, whilst the addend $RT \ln(\Omega_{n,i-1}/\Omega_{n,i})$ represents the statistical effect.

The interaction energy $\Delta G_{I,ij}$ per site, is defined as the difference in the intrinsic free energies of association of the jth and ith ligands:

$$\Delta G_{I,ij} = -RT \ln(K_i/K_j) + RT \ln\left(\frac{\Omega_{n,i-1}/\Omega_{n,i}}{\Omega_{n,j-1}/\Omega_{n,j}}\right) \tag{24}$$

On the basis of this definition of $\Delta G_{I,ij}$, if the j-th ligand binds more strongly than the ith, then as in cooperative systems, $\Delta G_{I,ij} < 0$. For the binding of O_2 to the haemoglobin [35], the Eq. (24) gives $\Delta G_{I,ij} = -2$ kcal per (mole site) for $i=1$ and $j=4$. This fact means that site–site interactions in this system have positive cooperativity.

For the purpose of treating and characterizing data on the cooperative association of ligands, it is common practice to use a semi-empirical approach and then to interpret the physical significance of the empirical parameters that are obtained.

Particularly, the parameter n_H or Hill constant [3] is introduced in the equations for a class of independent sites in terms of saturation ratio Y or the B/[L] ratio:

$$Y = \frac{[L]^{n_H}/K^{n_H}}{1 + ([L]^{n_H}/K^{n_H})} \tag{25}$$

$$\frac{B}{[L]} = \frac{n[L]^{n_H-1}/K^{n_H}}{1 + ([L]^{n_H}/K^{n_H})} \tag{26}$$

In these equations, K is the apparent dissociation constant for the interacting sites, n indicates the maximum number of ligand molecules that can be bound to the receptor. The Hill constant, n_H, gives the cooperativity degree: values between 0 and 1 indicate a negative cooperativity, whilst a positive cooperativity is observed for $1 < n_H < n$. Obviously, $n_H = 1$ means absence of interactions; otherwise, the theoretical possibility $n_H = n$ represents infinite cooperativity (or perfect cooperativity).

This type of approach was widely used to study the association events between cations and nucleic acids [35,52].

Because n_H can be written as:

$$n_H = \frac{d(\ln Y/(1-Y))}{d(\ln[L])} \tag{27}$$

its value can be obtained easily from the slope of the binding curve depicted in a Hill plot. Due to the strong dependence of this parameter from Y values, generally [35] it is evaluated at $Y = 1 - Y = 0.5$. For positive cooperativity, the Scatchard plot describes a curve which passes from the origin, with a maximum at $B_{max} = n(n_H - 1)/n_H$ and with an intercept on the B axes equal to n.

2.3.3. The homogeneous lattice systems (or sequential)

This type of model, introduced by Crothers [53] and developed by McGhee and von Hippel [40], is applied to the systems where the substrate contains a large amount of repeating site units (homogeneous lattice). Indeed, typical situations for the application of this model are constituted by proteins, histones, polyamines and different drugs bound to polynucleotides (DNA or RNA), or similarly by small molecules bound to polymers (peptides, polysaccharide, etc.).

It is assumed that the substrate is constituted by N identical repeating units (Fig. 5), oriented in a particular direction, this means we hypothesise polarity inside the lattice. The residues of this backbone structure could be associated with bases such as phosphates belonging to

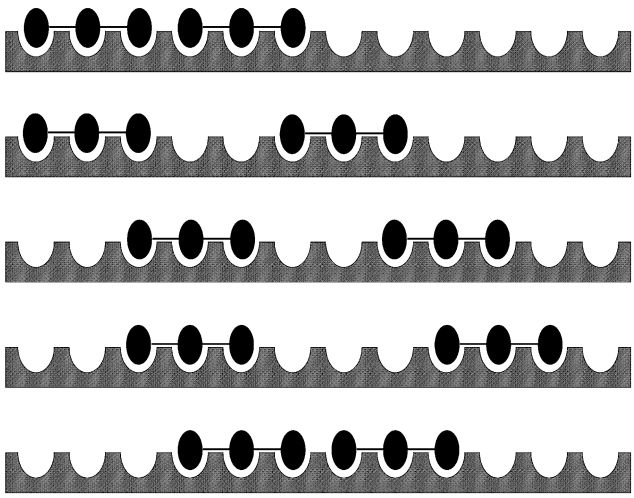

Fig. 5. Possible micro-species for the case of two ligands bound to the lattice with $l = 3$ and $N = 12$ (adapted from Ref. [35]).

nucleic acid, or to aminoacids or sugars belonging to the relative polymers. Furthermore, the ligand L has to occupy l consecutive lattice units. Moreover, the end chain effects can be supposed as negligible when $l \ll N$ (infinite lattice). Under these assumptions there are $N-l+1$ potential sites in the lattice. It is this aspect of the lattice that gives rise to a Scatchard plot markedly different from those obtained from other models.

As usual, the aim is to obtain an equation able to correlate the binding parameters (k, l and ω, the cooperativity parameter) to the macroscopic variables B and L. In this model, treatment was performed on the basis of statistical considerations. Fig. 5 illustrates the statistical complexities of the lattice for the case of $N = 12$ and $l = 3$.

B/[L] depends on the ratio between the average number of free ligand sites of length l per lattice, N_{fl}, and the intrinsic microscopic dissociation constant, k. N_{fl} is given by the following equation:

$$N_{fl} = N p_f (p_{ff})^{l-1} \tag{28}$$

where p_f is the probability that a lattice unit selected at random is unoccupied and p_{ff} is the conditional probability that a given free unit is followed by another free unit.

The ratio B/[L] could also depend from the cooperativity parameter ω, which is defined as the equilibrium constant for the ligand–ligand interaction in the lattice.

Let us consider two partially saturated lattice configurations for the ligand–lattice system (called configuration I) characterised by the following properties (see also Fig. 6):

1) On the left side of the lattice, an arbitrary distribution (A) of bound ligands exists with an end bound ligand.
2) On the right side of the ligand, there are: x free sites of the lattice; a bound ligand; and, subsequently, y free sites. If $x, y \geq 1$, the ligands are considered isolated.
3) On the right side of (A) there is a second arbitrary distribution (B) of ligands.

The second configuration (indexed II) is identical to I except from the reciprocal position of the two ligands that in this case are contiguous (see Fig. 6).

With these assumptions:

$$\omega = \text{probability (II)/probability (I)} \tag{29}$$

and its value is 1 for non-cooperative systems, < 1 if the closeness of the two ligands is unfavourable (negative cooperativity) and > 1 for positive cooperativity.

2.3.3.1. No ligand–ligand interactions ($\omega = 1$). In this case:

$$p_f = 1 - l\frac{B}{N}, \tag{30}$$

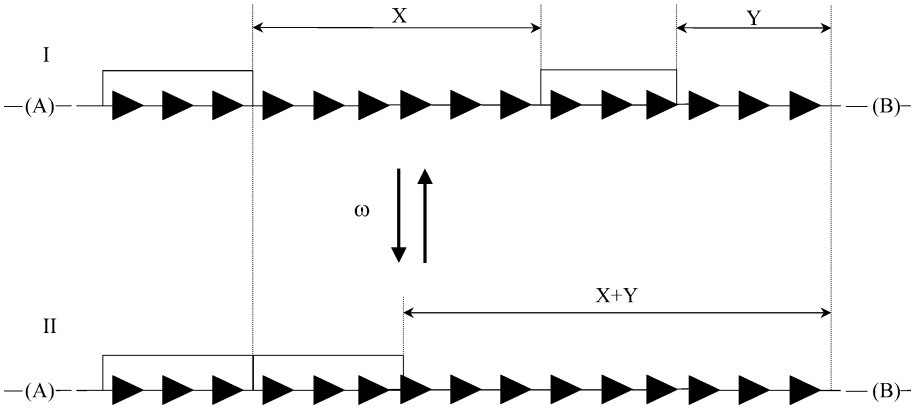

Fig. 6. Geometrical representation of the equilibrium constant for the ligand–ligand interactions. x and y indicate the empty lattice segments [40].

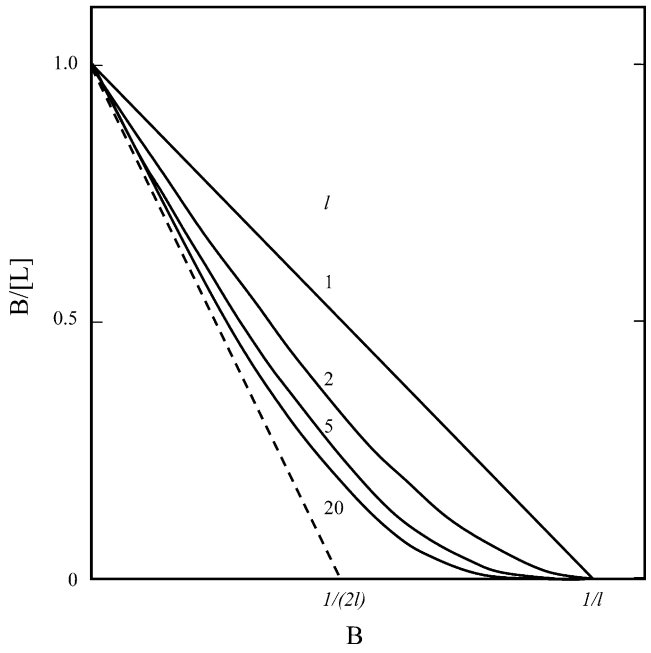

Fig. 7. Scatchard plots of ligand binding to a lattice for various values of l with $K = 1$ M (adapted from Ref. [40]).

$$p_{ff} = \frac{1 - l(B/N)}{1 - (l-1)(B/N)} \tag{31}$$

and

$$\frac{B}{[L]} = \frac{N}{k}(1 - l(B/N))\left(\frac{1 - l(B/N)}{1 - (l-1)(B/N)}\right)^{l-1}. \tag{32}$$

From Eq. (32) the following information is derived:

1) if $l = 1$ Eq. (32) becomes Eq. (15);
2) if $l \geq 2$ the last term is < 1 and it is function of B and l. Therefore, the resulting Scatchard plot will show non-linear behaviour with an upward convexity (Fig. 7);
3) the intercept on the B/[L] axis will be N/k;
4) the intercept on the B axis will be N/l (full saturation). For $l > 5$, a non-linear behaviour is expected which tends to a plateau as B/[L] decreases. In this case, the graphical extrapolation of the data could over-estimate the l value. It is considered that the barely detectable slope of the Scatchard plot in this region is generated from the accumulation of intervals in the lattice with dimension smaller than l. Otherwise, another interpretation suggests that these events are associated with the decrease of the mixing entropy which happens when the ligands in the lattice diffuse in order to allow the subsequent binding.
5) if the lattice contains more than one type of site, the resulting binding equation contains the sum of the binding equation for each type of site;
6) for a finite lattice, Eq. (32) has to be corrected by the factor $(N-l+1)/N$. For $N/l \geq 30$, Eq. (32) follows for chains endowed with a finite length.

2.3.3.2. Cooperative ligands. In this case three situations are taken into account (Fig. 8):

1) binding of an isolated ligand: the equilibrium constant is k;
2) binding of a ligand to a site contiguous to another one already bound: the equilibrium constant is $k\omega$;
3) binding of a ligand to a site contiguous to two others full sites: the equilibrium constant is $k\omega^2$.

This approach is similar to that proposed by Schwartz [54] who at first introduced the cooperativity parameter q. Some authors suggested the so-called 'limited cooperativity'. In this case the contribution of the term $k\omega^2$ is negligible.

The statistical treatment of a cooperative system (positive or negative) yields an equation for B/[L] which includes the three cases described above:

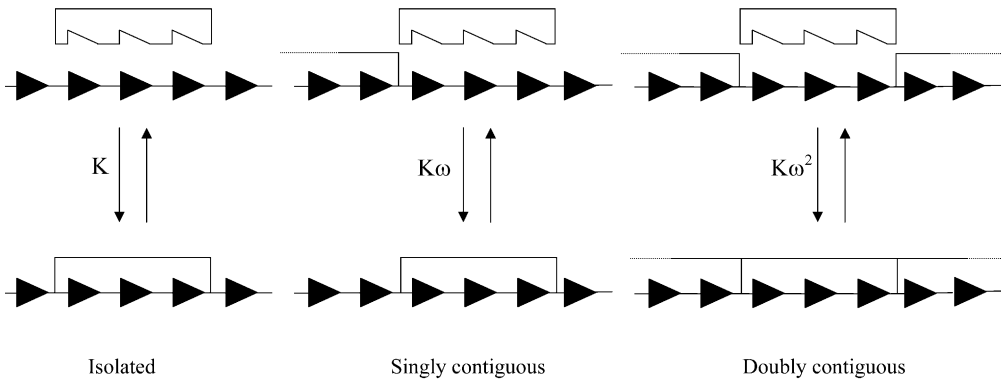

Fig. 8. Three hypothetical types of cooperative binding sites [40].

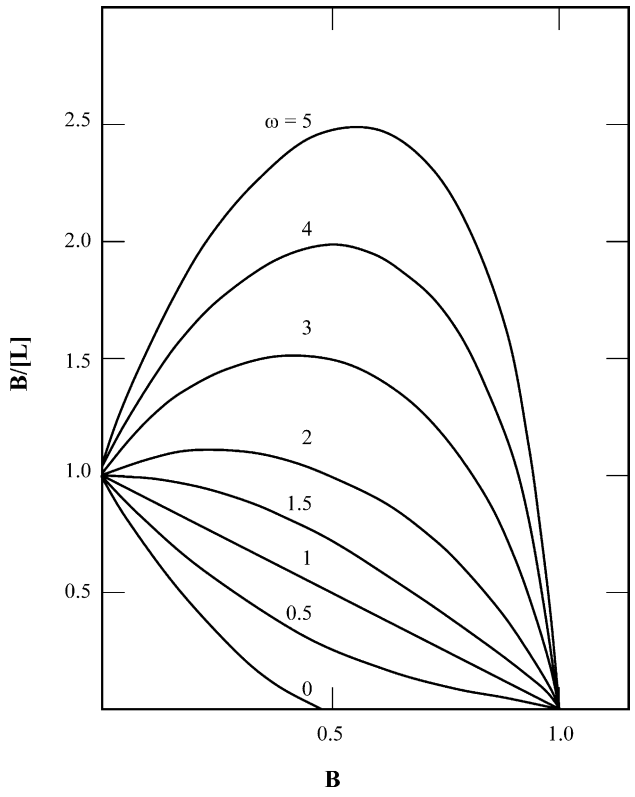

Fig. 9. Scatchard plots for ligand binding to a homogeneous lattice, for $K=1$ M, and $l=1$, with various values of the cooperativity parameter ω (adapted from Ref. [40]).

$$\frac{B}{[\mathrm{L}]}=\frac{N}{k}(1-l(B/N)) \times\left[\frac{(2\omega+1)(1-l(B/N))+(B/N)-R}{2(\omega-1)(1-l(B/N))}\right]^{l-1} \times\left[\frac{1-(l+1)(B/N)+R}{2(1-l(B/N))}\right]^{2} \quad (33)$$

where

$$R=\sqrt{[1-(l+1)(B/N)]^2+(4\omega(B/N))(1-l(B/N))}.$$

Eq. (33) is general and for $\omega=1$ gives Eq. (32).

When $\omega<1$, (anticooperative binding) Scatchard plots fall below those of non-interacting case. When $\omega=0$, (infinite anticooperativity) Eq. (33) reduces to Eq. (32) for non-interacting ligands with a length of $l+1$ segments. If $\omega>1$, the Scatchard plots are concave-down. Particularly, for $\omega>l+1/2$ the plot shows a maximum whose height increases with increasing ω (see Fig. 9).

For $l=1$ no 'overlap' effect mixed with the cooperativity is observed and the non-linearity in Scatchard plots is considered to be only due to the ligand–ligand interactions.

High l values generally explain anticooperativity in terms of curve profiles which are a compromise between the effects of l and ω. If ω is sufficiently high with respect to l, (about 10 times higher), the behaviour of the plot will be determined by the ω/l ratio and the maximum will be between the limits $N\omega/2l$ and $N\omega/l$.

In any case in the Scatchard plots, the intercepts on the axes coincide with those obtained for a non-interacting system. Clearly, if $\omega>1$ the intercept on the x-axis will be easier to determine with respect to the other cases where the presence of entropy effects inhibits the saturation of the system giving so rise to an asymptotic decrease of $B/[\mathrm{L}]$.

Also in this case, it is possible to obtain a Scatchard equation for a receptor with more classes of sites. Its general form is:

$$\frac{B}{[\mathrm{L}]}=\sum_i(i\text{th site binding constants}) \times(\text{number of available sites}) \quad (34)$$

This model is widely used to investigate binding events in the field of molecular biology.

Actually, the McGhee and von Hippel model has been widely used to study the Scatchard curves of systems containing nucleic acids [55–58]. However, in the literature, when a downward convexity is detected, the application of the Eq. (32) was preferred instead of the parameter ω, in order to obtain an 'apparent length of the site' which so includes any cooperative effect [59–61].

2.3.4. Thermodynamic model

The thermodynamic model proposed by Di Noto et al. [23,34], is useful to fit the binding data because it allows us to analyse binding experiments in a very generalised way and it is easy to handle. This general approach is suitable to investigate receptor–ligand

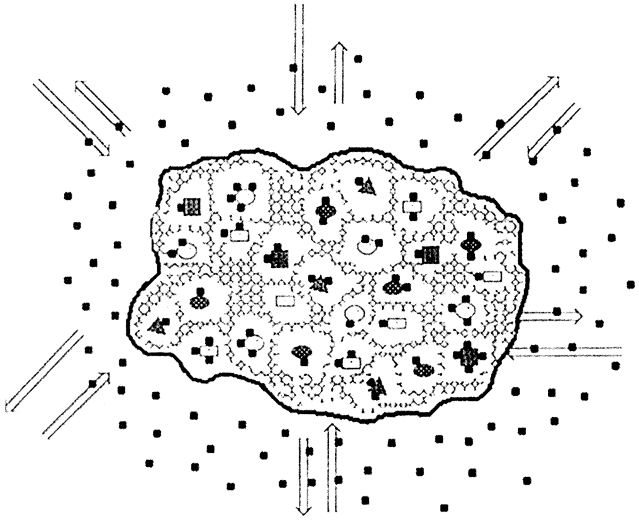

Fig. 10. Model for the receptor–ligand interactions. The receptor includes groups of different types of binding sites each of which may exhibit multiple occupancies [23].

systems where, during the binding process, conformational changes can occur, so that the affinity of the ligand towards some chemical sites could continuously be modified. These phenomena are usually considered as cooperative events [54], and could be evaluated on basis of non-equilibrium thermodynamics [62]. Otherwise, it is straightforward to reduce the general equations to those describing the binding processes previously discussed.

In Fig. 10 a possible receptor having s types of sites is depicted; these sites can bind until n_i ligands (if $n_i > 1$ multiple coordination to ith site is expected); the different levels of multiple coordination are singled out by l index.

It is assumed that the free energy change of the system, due to the binding or the release of a mole of ligand from the ith site, promotes the binding experiment. In this case:

$$\mathrm{d}G = \sum_{i=1}^{s} \sum_{l=1}^{n_i} [\mu_{i,l}^{S} + \mu_{i,l-1}^{R} - \mu_{i,l}^{R}]\mathrm{d}\xi$$

$\mu_{i,l}^{S}$, $\mu_{i,l}^{R}$, $\mu_{i,l-1}^{R}$, are the chemical potentials for the ith site with a coordination that varies from l and $l-1$. The S index refers to the change in the system of free energy due to binding or release of a mole of free ligand. The R index refers to the same change, but consequent to the molar change in the receptor at the ith site endowed with multiple coordination l or $l-1$. $\mathrm{d}\xi$ is the infinitesimal extent of reaction. In this treatment it was assumed that the concentrations of the species in solution are coincident with their activities and that the reaction rate for the k-th site with j-th coordination is time depending [62,63].

From the $\mathrm{d}G$ equation one obtains:

$$[B] = \sum_{i=1}^{S} [B_{\max,i}] \left\{ \frac{\sum_{k=1}^{n_i} [F]^k \Big/ \prod_{j=1}^{k} K_{i,j}(t)}{1 + \sum_{k=1}^{n_i} [F]^k \Big/ \prod_{j=1}^{k} K_{i,j}(t)} \right\}. \quad (35)$$

If we consider the maximum ligand concentration bound to the ith site as:

$$[b_{\max,i}] = [A_{i,0}] + \sum_{k=1}^{n_i} k[A_{i,k}] = [A_{i,0}] + [b_i] \quad (36)$$

similarly to Eq. (35), we can obtain:

$$[b] = \sum_{i=1}^{S} [b_{\max,i}] \left\{ \frac{\sum_{k=1}^{n_i} k\left([F]^k \Big/ \prod_{j=1}^{k} K_{i,j}(t) \right)}{1 + \sum_{k=1}^{n_i} \left([F]^k \Big/ \prod_{j=1}^{k} K_{i,j}(t) \right)} \right\} \quad (37)$$

From this relationship the Adair Eq. (16) can easily be derived. It was proven that, if the binding experiment is performed in the mono-coordination regime for each type of site (i.e. when the concentration of multiple coordination sites is lower than that of mono-coordination sites), Eqs. (35) and (37) are coincident. This condition should be fulfilled in order to determine realistic binding parameters from the experimental data [23].

Eq. (35) allows us to derive a very general relationship for the Scatchard plots:

$$\frac{[B]}{[F]} = \sum_{i=1}^{S} ([B_{\max,i}] - [B_i]) \times \left[1/K_{i,l}(t) + \sum_{k=2}^{n_i} \left([F]^{k-1} \Big/ \prod_{j=1}^{k} K_{i,j}(t) \right) \right]. \quad (38)$$

Let us assume:

$$[B_{\max,i}] - [B_i] = x_i(F)([B_{\max}] - [B]) = V_i(F) \quad (39)$$

where $x_i(F)$ is the molar fraction that may be bound in the ith site (fractional 'empty' ith sites) [23], it is straightforward to obtain

$$x_i = \frac{1}{1 + \sum_{j=1,\, j\neq i}^{S} [V_i(F)]^{-1} V_j(F)}. \quad (40)$$

Briefly, x_i can be written as follows

$$x_i = \frac{1}{1 + \beta_i[F]} \quad (41)$$

where

$$\beta_i = \frac{1}{V_i(S_0)} \sum_{j=1_{j\neq i}}^{S} V_j\, V_j(S_0). \quad (42)$$

$[S_0]$ is the initial ligand concentration, β_i [mol^{-1}], is a parameter which accounts for the influence of the parallel filling of the other jth sites with respect to the ith site. Thus, β_i can be considered as a cooperativity factor for the ith site.

On these bases, Eq. (38) yields:

$$\frac{[B]}{[F]} = \sum_{i=1}^{S} \left(\frac{[B_{\max}] - [B]}{1 + \beta_i[F]} \right) \times \left[\frac{1}{K_{i,1}(t)} + \sum_{k=2}^{n_i} \left([F]^{k-1} \Big/ \prod_{j=1}^{k} K_{i,j}(t) \right) \right]. \quad (43)$$

This latter equation is an explicit function of the implicit Eq. (34), suggested by McGhee and von Hippel [40] for a general system with many sites. $([B_{\max}] - [B])$ corresponds to the number of sites potentially available for binding, $1/(1 + \beta_i[F])$ can be associated with the cooperativity parameter ω, and the term in square brackets is a factor including the binding constants of the system.

By combining Eqs. (41) and (43), an equation, similar to that already known for the Hill constant, is given:

$$n_H = \frac{d\{\ln([B]/[B_{max}] - [B])\}}{d(\ln[F])} \quad (44)$$

from which a general equation for the Hill profiles is derived:

$$\ln\left\{\frac{[B]}{[B_{max}] - [B]}\right\} = \ln\left\{\sum_{i=1}^{S}\left(\frac{[B_{max}] - [B]}{1 + \beta_i[F]}\right) \times \left[\frac{1}{K_{i,1}(t)} + \sum_{k=2}^{n_i}\left([F]^{k-1} \Big/ \prod_{j=1}^{k} K_{i,j}(t)\right)\right]\right\} + \ln[F]. \quad (45)$$

Finally, the overall binding constant L(F) of the ligand–receptor system is:

$$L(F) = \frac{[B]}{([B_{max}] - [B])[F]} \quad (46)$$

which depends on the difference of standard overall free energy during the experiment as follows:

$$\Delta G = -RT \ln(L(F)), \quad (47)$$

thus indicating that ΔG depends on the free ligand concentration.

2.3.4.1. Simulations. To study the profiles of the binding relationships described above, simulations under the following conditions and a fixed time t, have been carried out:

a) two types of monocoordinated sites, having $1/K_{1,1} = 0.12$ (a.u.) and $1/K_{2,1}$ ranging between 0.0048 and 0.12 (a.u.). If the two binding constants are coincident, the equation describes a system with only one type of monocoordinated site;
b) two types of sites with double coordination: in this case $K_{i,1}$ values are assumed as in (a), whilst $K_{i,2} = 0.1\%\ K_{i,1}$;
c) two types of sites with double coordination: the $K_{i,1}$ as in (a) and $K_{i,2} = 1\%\ K_{i,1}$;
d) two types of sites with double coordination: the $K_{i,1}$ as in (a) and $K_{i,2} = 50\%\ K_{i,1}$.

Simulations were performed with binding variables $[F]$ and $[B]$ ranging in $0 \le [F] \le 5000$ (a.u.) and $0.5 \le [B] \le 22$ (a.u.) units, respectively.

2.3.4.1.1. Simulated Scatchard profiles. The Scatchard profiles (Fig. 11), which have been derived from Eq. (43) for a receptor characterised by two types of sites, show that, if the receptor has only one mono-coordinated site, the classical Scatchard linear behaviour is obtained. The presence in the receptor of two types of sites with single coordination provides profiles with upward convexity, similar to those observed for more classes of indepen-

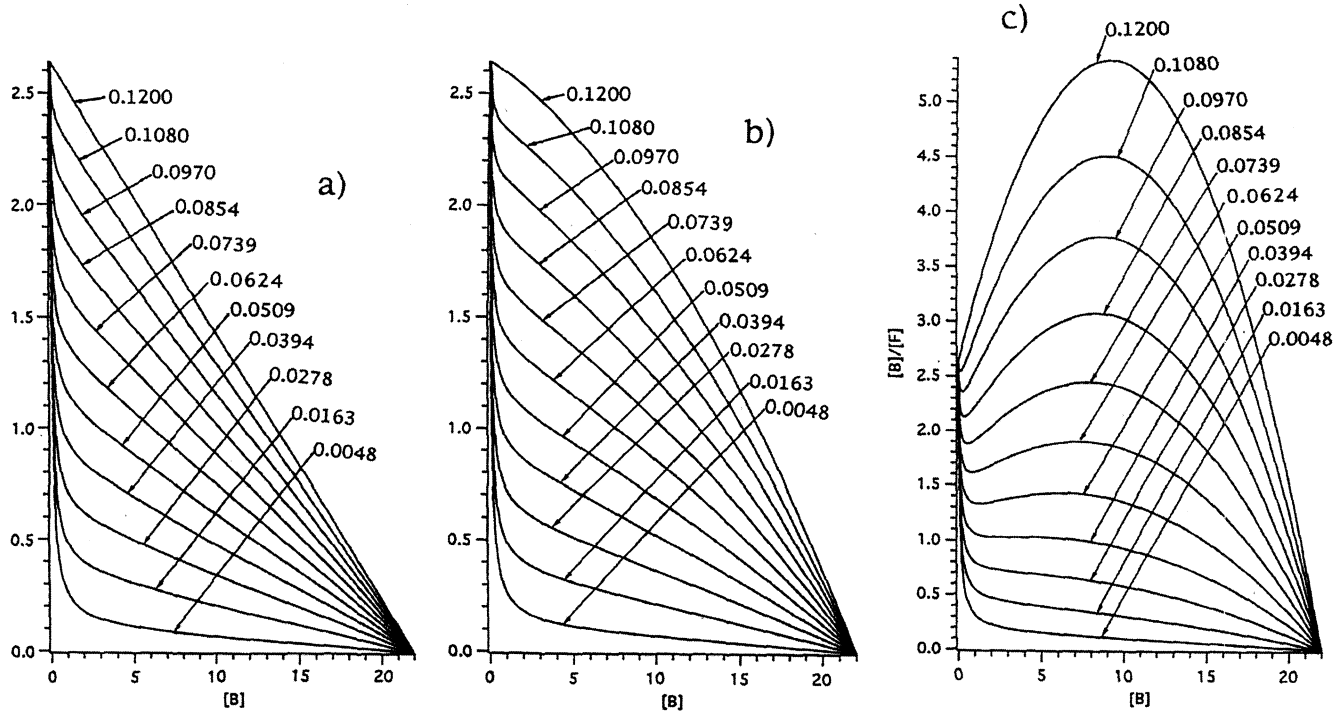

Fig. 11. Simulated Scatchard plots for a receptor having two types of sites. The profiles were calculated assuming that $1/K_{1,1}$ is constant at the value of 0.12 (a.u.) and $1/K_{2,1}$ is varied in the range $4.8 \times 10^{-3} \le 1/K_{2,1} \le 0.12$ (a.u.), the values are reported in the figures; $[B]$ and $[F]$ change in the ranges $0 \le [F] \le 5000$ (a.u.) and $0.5 \le [B] \le 22$ (a.u.), respectively. Simulations performed with Eq. (38): (a) without multiple coordination; (b) assuming values for the double-coordination binding constant of 0.1% (b); 1.0% (c) of the value of the single coordination constant.

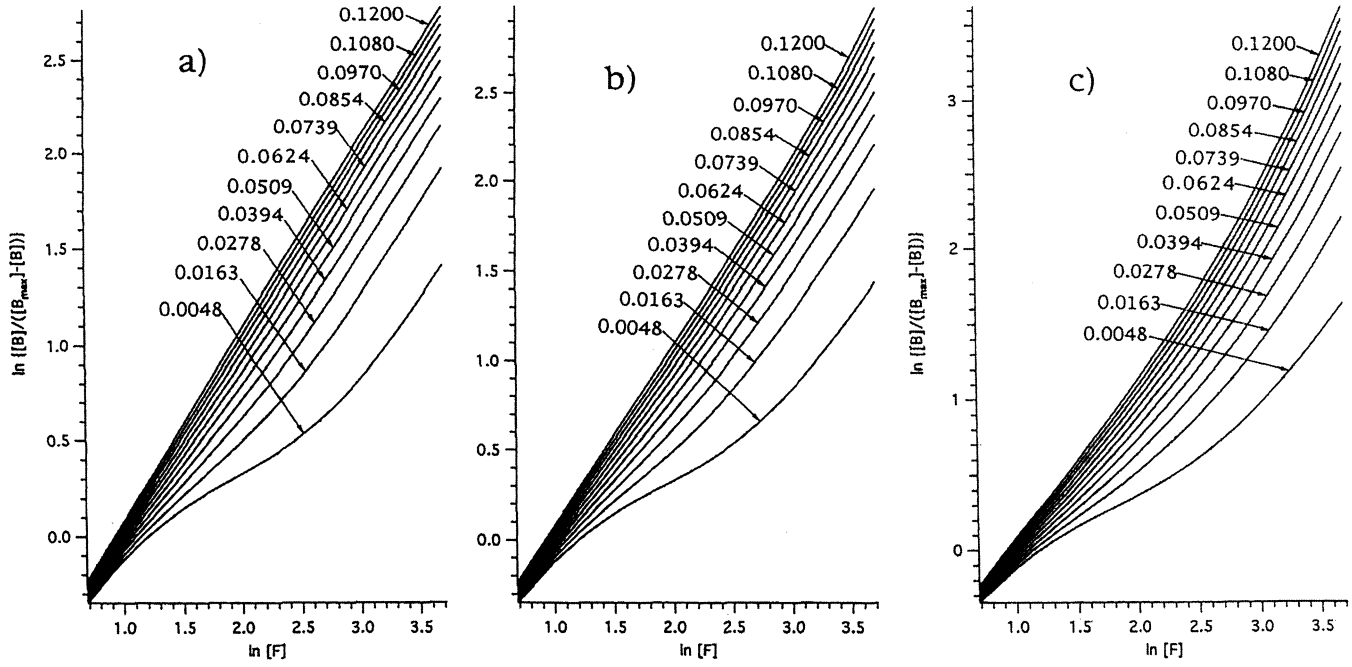

Fig. 12. Simulation of Hill plots with Eq. (45). Calculation conditions as in Fig. 11. (a) Without multiple-coordination; (b, c) with double-coordination (calculation conditions as in Fig. 11) [23].

dent sites in the classical approaches. If multiple coordination occurs, an inversion of convexity for high values of B is revealed (i.e. in the experimental conditions near to the saturation or when the majority of the sites are mono-occupied). This behaviour becomes more significant if both the ratio between the first and second dissociation constants and the difference between $K_{i,1}$ decrease.

2.3.4.1.2. Simulated Hill profiles. The Hill plots relative to the different situations above described have been obtained from Eq. (45) and show the following properties (Fig. 12):

1) One type of monocoordinated site: the plot is linear, with slope equal to unity (this confirms classical behaviour).

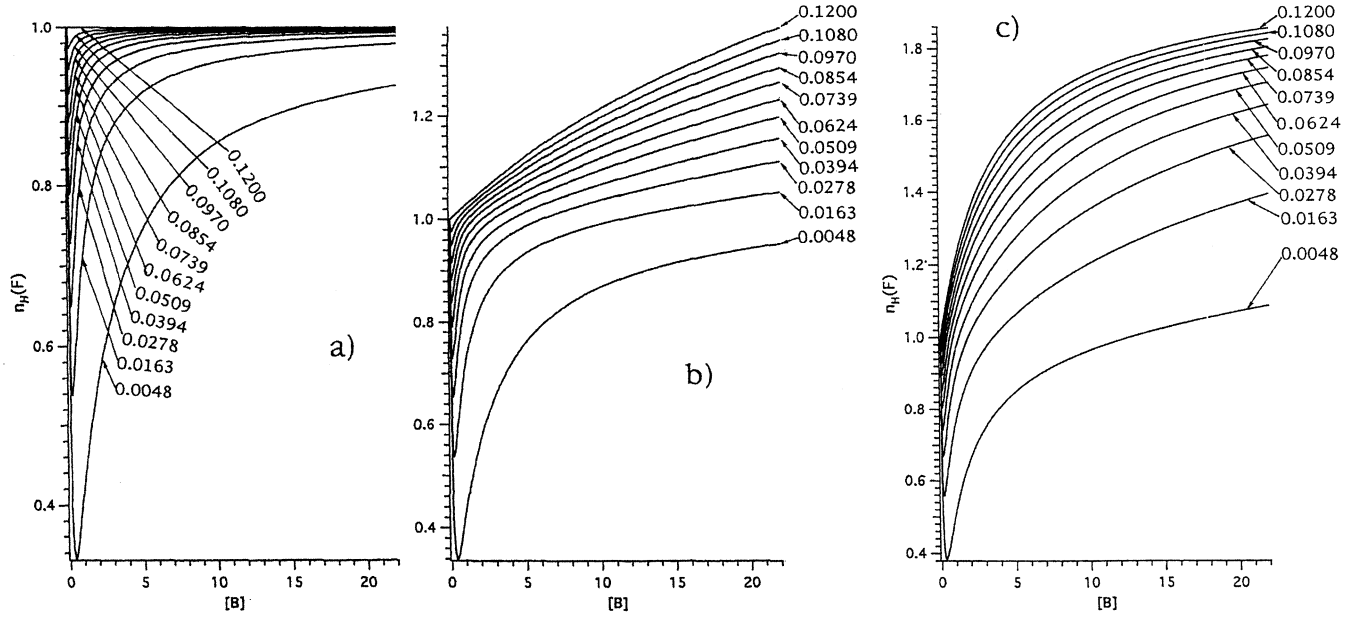

Fig. 13. Simulations of $n_H(F)$ factor on $[B]$ using Eq. (44). (a) Without multiple-coordination; (b, c) with double-coordination (calculation conditions as in Fig. 11) [23].

2) Two types of monocoordinated sites: an overall non-linear profile is observed, characterised by unitary slopes for very high or very low [B] values.
3) Two types of double coordinated sites: the behaviour is similar to the previous one, but slopes different from the unity are observed in the linear regions for values very high or very low [B].

The shapes of the curves obtained from this type of approach are less informative when compared with the corresponding Scatchard plots.

2.3.4.1.3. Simulated $n_H(F)$ profiles. The curves of Hill coefficient, $n_H(F)$, as a function of [B] are depicted in Fig. 13.

1) For a system with two mono-coordinated sites $0 \geq n_H \leq 1$. If the difference between the values of $K_{i,1}$ constants decreases, n_H tends to unity (in other words the two types of site are not clearly distinguishable). The n_H differences depend directly on β_1. It is clear that in the presence of only one type of site, the n_H value is constant and equal to 1, according to the systems where cooperative events are absent ($\beta_1 = 0$).
2) In the case of a receptor with two double-coordinated sites, when the influence of multiple coordination to the overall binding process becomes significant, n_H tends asymptotically to 2, i.e. to the value of the multiple coordination. This behaviour is observed both with decreasing difference between the $K_{i,1}$ values, and when the second association constant becomes comparable to the first one.

These results are in agreement with those reported in the literature [1,35,64] and suggest that this latter model yields a rigorous thermodynamic basis which explains in a coherent way the non-linear profiles frequently observed in the experimental Scatchard, Hill and Adair plots. Moreover, this thermodynamic model shows that the empirical relationships mentioned above are specific simplifications of the more general Eq. (35) which may be applied to experiments at equilibrium or not at equilibrium.

Results summarised in Table 1 allows us to carry out, a qualitative analysis of the system (in detail, to gain the minimum number of sites and their type of coordination) simply by taking into account the behaviour of Scatchard profiles. This preliminary analysis is very advantageous in order to carry out accurately the following quantitative treatment of the binding data, thus permitting us to select the most suitable equations for the interpolation of the experimental data by fitting procedures. These latter calculations will provide, by using Eqs. (35), (43) and (45) the [B_{max}], [$B_{max,i}$] and $K_{i,j}$ parameters and the dependence of mole fraction, $x_i(F)$, on [F] and [B]. Finally the use of Eq. (47) yields a measure of the standard free energy changes which occur during the ligand–receptor binding process.

3. Binding studies of the Al(III)–trypsin and DL-DPPC liposomes systems

In this section the thermodynamic model elucidated above (Section 2.3.4) and widely applied in the investigation of binding between natural polyamines and rat liver mitochondria [65–68], is used to fully characterize the response induced in trypsin and DPPC liposomes by the external concentration of Al(III) species. These studies could be of fundamental importance to disclose the molecular mechanisms of Al(III) species toxicity.

3.1. Materials and methods

3.1.1. Material preparations

DL-DPPC (Sigma) liposomes were prepared as described elsewhere [69]. Briefly, DPPC was solubilized in 95% ethanol under moderate stirring, and injected by a microsyringe into a buffered solution at 70 °C. Liposomes suspension was then liophylized against Tris–HCl $I = 0.1$, pH 7.5.

Trypsin (Sigma) solution was prepared at a concentration of 2 mg ml^{-1} in Tris–buffer solution, $I = 0.1$, pH 7.5.

Al^{3+} analysis either in liposomes suspensions or in trypsin solution after equilibrium dialysis experiments was carried out as described elsewhere [70].

3.1.2. Equilibrium dialysis

Eleven cylinders containing each 100 ml of Tris–HCl buffer, $I = 0.1$ and pH 7.5, were utilized to dialyse 3 ml

Table 1
Summary of the curve shapes and features obtained by numerical simulations of Eqs. (38), (45) and (44)

Site types	Coordination	Scatchard	Hill	n_H
1	Single	Linear-plot	Linear-plot	1
Many	Single	Hyperbolic like-plot with upward convexity	Non-linear plot with a slope tending to unity at very high and very low ln[F]	$0 \leq n_H \leq 1$
Many	Multiple	Hyperbolic like-plot with downward convexity	Non-linear plot with a slope different from unity in the linear region of the plot	$0 \leq n_H \leq 2$

of the liposome suspensions or trypsin solutions (2 mg ml^{-1}) in Visking dialysis bags at room temperature for 24 h. At first the Visking dialysis bags were equilibrated with a 10 mM desferoxamine (Sigma, Milan, Italy) solution in order to remove all traces of Al(III). Desferioxamine solution was then substituted with Tris–HCl buffer $I = 0.1$, pH 7.5 at room temperature for three times. Afterward, 100 ml of Tris–HCl buffer, containing varying quantities of AlLac3, starting with AlLac3 10 mM solution, were placed in each separated cylinder for 24 h at room temperature. Finally the unbound metal was removed by exhaustive dialysis against Tris–HCl buffer.

3.1.3. Al(III) analysis

The amounts of Al in the samples were determined by inductively coupled plasma atomic emission spectrometry (ICP-AES) using the Spectroflame Modula spectrometer equipped with an ultrasonic nebulizer, Model USN-100 from Spectro Analytical (Kleve, Germany). The Al determination was performed using the emission line at 308.215 nm, a plasma power of 1.2 kW, a radiofrequency generator of 27.12 MHz and an argon gas flow in the nebulizer, auxiliary and coolant of 1, 0.5 and 14 l min^{-1}, respectively. The USN operated with a sample flow rate of 2.0 ml min^{-1} and desolvation and condensation temperatures of 140 and 4 °C, respectively.

Solutions suitable for ICP-AES analysis were obtained by microwave sample digestions carried out using a CEM MSD-2100 microwave sample preparation system. The analyses were performed using the method of standard additions.

3.1.4. Calculation methods [65–68]

Binding parameters and consequent energies were determined by using Eq. (43) for Scatchard and Eq. (45) for Hill analysis. After that, $[B_{max,i}]$, the maximum ith sites concentrations that may be bound by ligand, were determined by fitting Eq. (35) on the $[B]$ and $[F]$ plots. The fits were performed using a Fortran program developed in our laboratory. This realizes the minimization by using the Minuit subroutine [71] which is called from the main program. The program was written in Microsoft Fortran Power Station (Professional Development System Ver. 1.0). The distribution of total bound Al(III) on their respective binding sites has been determined by parameter $x_i(F_i)$. This parameter was calculated using Eqs. (39) and (41).

3.2. The Al(III)–trypsin system

The results reported in Fig. 14(a) show that Al(III) uptake by the trypsin enzyme increases as the protein is equilibrated with increasing Al(III) concentration. Fig. 14(b) depicts the binding data in the Scatchard repre-

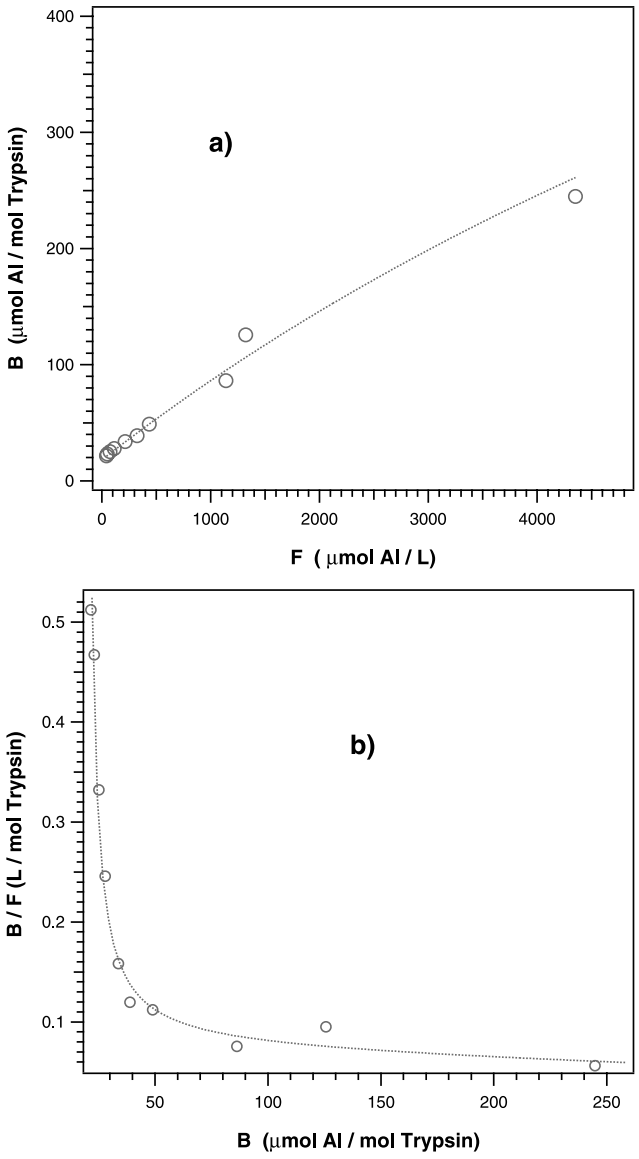

Fig. 14. Al(III)–trypsin binding process. (a) Dependence of $[B]$ on $[F]$, the dotted line was obtained by fitting Eq. (35) to the experimental data (open circles); (b) experimental Scatchard plot, the dotted curve was obtained by fitting Eq. (38) to the data (open circles).

sentation. The data in this plot exhibit a typical hyperbolic like behaviour with upward convexity indicating on the basis of Table 1, that in trypsin many types of sites with single coordination could be present. The dotted lines in the plots of Fig. 14(a and b) show the fitted curves obtained as described in Section 3.1.3 by using Eqs. (35) and (38), respectively. The parameters so determined were confirmed by fitting Eq. (45) to the Hill plot shown in Fig. 15(a). These analyses confirm a receptor having two types of binding sites S_1 and S_2 both with mono-coordination. In Table 2 are summarized the Al(III) binding parameters provided by the analysis of $[B]$ versus $[F]$, Scatchard and Hill data. Obviously, the fitting of Eqs. (35), (43) and (45) to the experimental

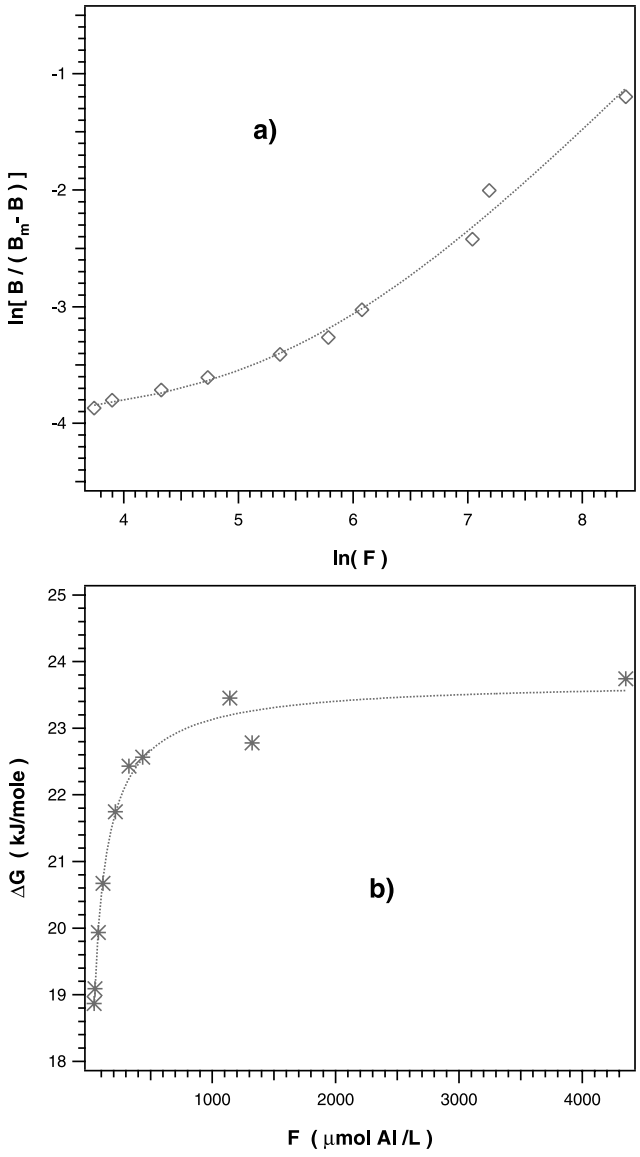

Fig. 15. Al(III)–trypsin binding process. Hill (a) and free energy (b) plots. Dotted lines were determined by fitting Eq. (45) (a) and Eq. (47) (b) to the experimental data.

data in terms of the above representations, gives the same parameters owing to the fact that they are generated from the same binding experiment and that Eqs. (43) and (45) are derived by the same general Eq.

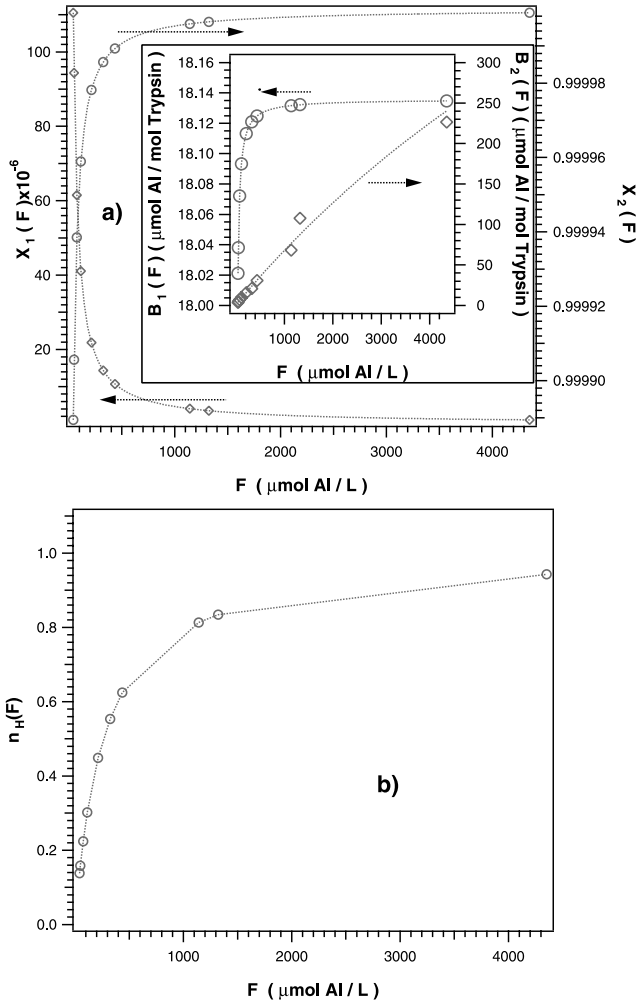

Fig. 16. Al(III)–trypsin binding process. Dependence on the free Al(III) species concentrations of the molar fractions $x_i(F)$ (a), and $n_H(F)$ (b).

(35). These investigations proved the presence in trypsin of two types of binding sites for Al(III). The total binding site concentration is 1056.6 (μmol/mol trypsin) distributed between S_1 and S_2 sites in the percentage of 2 and 98, respectively. The dissociation constants $K_{1,1}$ and $K_{2,1}$ of S_1 and S_2 sites, respectively, suggest that S_1 has a higher affinity than S_2. Indeed, $K_{1,1}$ is ca. 6×10^4 times lower than $K_{2,1}$. β_1 describes the possible influence of the parallel filling of S_2 on that of the S_1 site. Fig. 15(b)

Table 2
Aluminium–trypsin binding parameters determined by curve fitting of Eqs. (35), (43) and (45) in the data of [B] vs. [F], Scatchard and Hill plots, respectively

B_{max} (μmol Al/mol trypsin)	$B_{max,1}$ (μmol Al/mol trypsin)	$B_{max,2}$ (μmol Al/mol trypsin)	$K_{1,1}$ (μmol Al/L)	$K_{2,1}$ (μmol Al/L)	β_1 (μmol Al/L)$^{-1}$	χ [b]
1056.6(1) [a]	18.136(3)	1038.5(7)	0.2531(2)	$1.424(5) \times 10^4$	214.6(3)	0.0008273

[a] Standard deviations in the least significant digits are given in parentheses.
[b] χ indicates the goodness-of-fit.
$\chi = (\Sigma\ |(N_0)-(N_c)|)/(\Sigma\ |(N_c)|)$, where (N_0) is the experimental value and (N_c) is the calculated one. For a Scatchard plot, N is given by B/F and for a Hill plot by $\ln[(B)/(B_{max}-B)]$.

shows the functional dependence of the overall free energy changes (ΔG) on the concentration of free Al(III) in solution. ΔG was determined by means of the general Eq. (47).

The difference between the ΔG values obtained from $B=0$ to ∞ is comparable to that observed in other ligand–receptor binding investigations [35]. In Fig. 16(a) are reported the dependence on [F] of the molar fractions $x_1(F)$ and $x_2(F)$ for the aliquot of free Al(III) that can bind to S_1 and S_2 sites, respectively. These ratios are also named 'filling molar fractions'. The $x_1(F)$ values show that by enhancing the amount of bound Al(III), $x_1(F)$ diminishes and conversely, $x_2(F)$ increases. This means that the higher affinity S_1 site is filled before the S_2 site as confirmed in the inset of Fig. 16(a), where the amount of Al(III) bound to each site is plotted against [F] concentration. Furthermore, the concentration of Al(III) bound to S_1 site reaches saturation, while that bound to S_2 does not, even at the highest [F] values. This evidence indicates that the concentration of free Al in solution is able to trigger different trypsin–Al(III) complexes owing to the different binding capabilities of the two types of sites.

Finally, Fig. 16(b) reports values of the Hill factor $n_H(F)$ as a function of the amount of Al(III) bound to trypsin. The Hill factor was determined by means of Eq. (44) adapted for a system where two types of binding sites both with mono-coordination are present. For very low amount of bound Al(III) the Hill factor exhibits a value less than 1. This fact could demonstrate the existence of a very weak negative, cooperative effect under these conditions.

3.3. The Al(III)–DPPC liposomes system

In order to detect the number of binding sites in liposomes and their affinity toward Al, the system Al(III)–DPPC liposomes was studied in details as described in Section 3.2. Fig. 17(a) reports the binding curve which shows typical saturation behaviour. In Fig. 17(b) the Scatchard plot is reported. In agreement with Table 1, this could easily be attributed to a classical experiment where more than one type of site with mono-coordination is present in the receptor. Fig. 18(a) depicts the binding data for Al(III)–DPPC liposomes system in terms of the Hill representation, thus confirming the qualitative indications inferred from the Scatchard plot. The dotted lines in Fig. 17(a and b) and Fig. 18(a) were determined as described above by fitting the experimental data with Eqs. (35), (38) and (45), respectively. The binding constants so obtained are shown in Table 3. The results reveal the presence of two mono-coordinated binding sites on the DPPC liposomes, as found in the Al(III)–trypsin system. The total binding capacity in presence of Al of DPPC liposomes is 1.28 (μmol mol^{-1} liposomes), with 47 and 53% distributed between the S_1 and S_2 sites, respectively. The dissociation constants $K_{1,1}$ and $K_{2,1}$ of sites S_1 and S_2, respectively, indicate that the affinity of S_1 is about 169 times higher than that of S_2. Parameter β_1 exhibits, as is expected, a value lower than that observed for the Al(III)–trypsin system. Fig. 18(b) shows that the functional dependence of the overall free energy changes on the concentration of free Al(III) in solution occurs with a energy gap of about 9 kJ mol^{-1}. This value is about twice that observed for the Al(III)–trypsin system, suggesting that the binding of Al(III) to DPPC liposomes probably induces more significant structural effects with respect to those registered in the trypsin. Fig. 19(a) shows the molar fraction ratios $x_1(F)$ and $x_2(F)$ for the aliquot of free Al(III) that can bind to

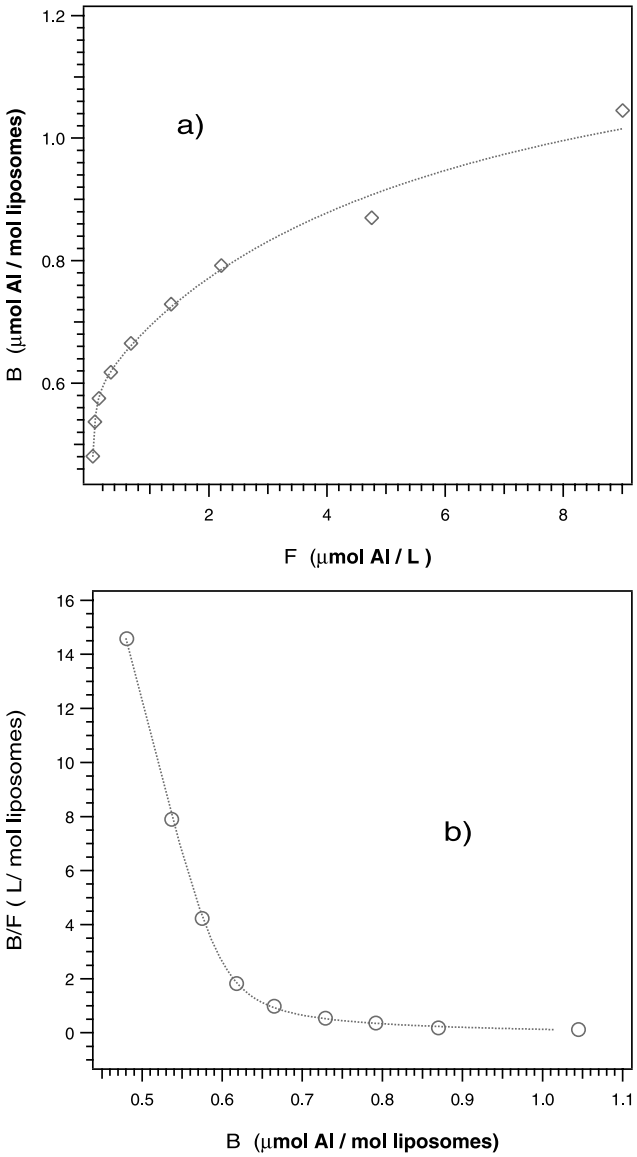

Fig. 17. Al(III)–DPPC liposomes binding process. (a) Dependence of [B] on [F], the dotted line was obtained by fitting Eq. (35) to the experimental data (open circles); (b) experimental Scatchard plot, the dotted curve was obtained by fitting Eq. (38) to the data (open circles).

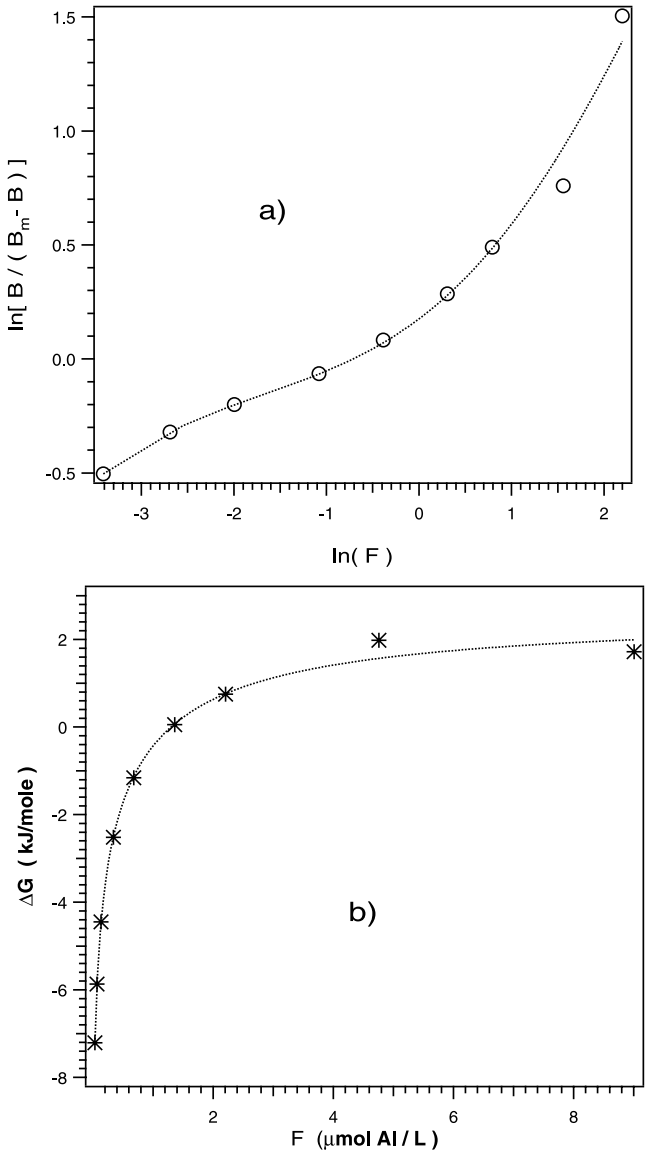

Fig. 18. Al(III)–DPPC liposomes binding process. Hill (a) and free energy (b) plots. Dotted lines were determined by fitting Eq. (45) (a) and Eq. (47) (b) to the experimental data.

sites S_1 and S_2, respectively. As previously observed for Al(III)–trypsin these values indicate that with increasing amounts of bound Al(III), $x_1(F)$ decreases and the opposite behaviour is observed for $x_2(F)$. Thus the S_1 site is filled before the S_2 site. However, as demonstrated by the inset of Fig. 19(a) the S_2 site begins to bind Al simultaneously to S_1 site and the amount of metal binding at first decreases as $[F]$ increases until a minimum is reached. After this minimum, as $[F]$ increases B_1 increases quite linearly. This behaviour was not observed in previous experiments. In agreement with these results, the Hill factor for the entire binding process exhibits values lower than unity (Fig. 19(b)). At low amounts of bound Al very low $n_H(F)$ values are observed (ca. 0.2). In accordance with the Al(III)–trypsin system the results also in this case indicate the possible existence of a weak negative cooperative effect in the Al(III)–DPPC liposomes interaction.

4. Final remarks

Ligand–receptor interactions are of fundamental importance in biochemical systems. In this paper we summarised some of the most useful formalisms which have been developed to investigate the equilibrium properties of the receptor–ligand systems that are commonly encountered. In such treatments it was important to highlight firmly to the reader the distinction between microscopic and macroscopic binding constants, and associated statistical features. Therefore, a general and rigorous thermodynamic treatment which explains in a coherent way the non-linear profiles observed in the empirical binding, Scatchard, Hill and Adair plots are briefly reported. This model shows that: (a) the empirical Scatchard, Hill and Adair functions are specific simplifications of a more general Eq. (35); and (b) that we can carry out qualitative and quantitative investigation on the Al species–receptor system binding process in a straightforward manner. Particularly, Table 1, which summarises the simulation results determined with this model, enables us to gain the first preliminary qualitative information on the type of binding process under investigation. This is done simply by observing the curve profiles and the convexity exhibited by the Scatchard and Hill experimental curves. On the other hand, by fitting procedures it is possible to determine the following binding parameters: (1) the coordination

Table 3
Aluminium–DL-DPPC liposomes binding parameters determined by curve fitting of Eqs. (35), (43) and (45) in the data of $[B]$ vs $[F]$, Scatchard and Hill plots, respectively

B_{max} (μmol Al/mol liposomes)	$B_{max,1}$ (μmol Al/mol liposomes)	$B_{max,2}$ (μmol Al/mol liposomes)	$K_{1,1}$ (μmol Al/L)	$K_{2,1}$ (μmol Al/L)	β_1 (μmol Al/L)$^{-1}$	χ [b]
1.28(1) [a]	0.594(6)	0.683(2)	0.0168(4)	2.8337(1)	69.35(5)	0.00154

[a] Standard deviations in the least significant digits are given in parentheses.
[b] χ indicates the goodness-of-fit.
$\chi = (\Sigma\ |(N_0)-(N_c)|)/(\Sigma\ |(N_c)|)$, where (N_0) is the experimental value and (N_c) is the calculated one. For a Scatchard plot, N is given by B/F and for a Hill plot by $\ln[(B)/(B_{max}-B)]$.

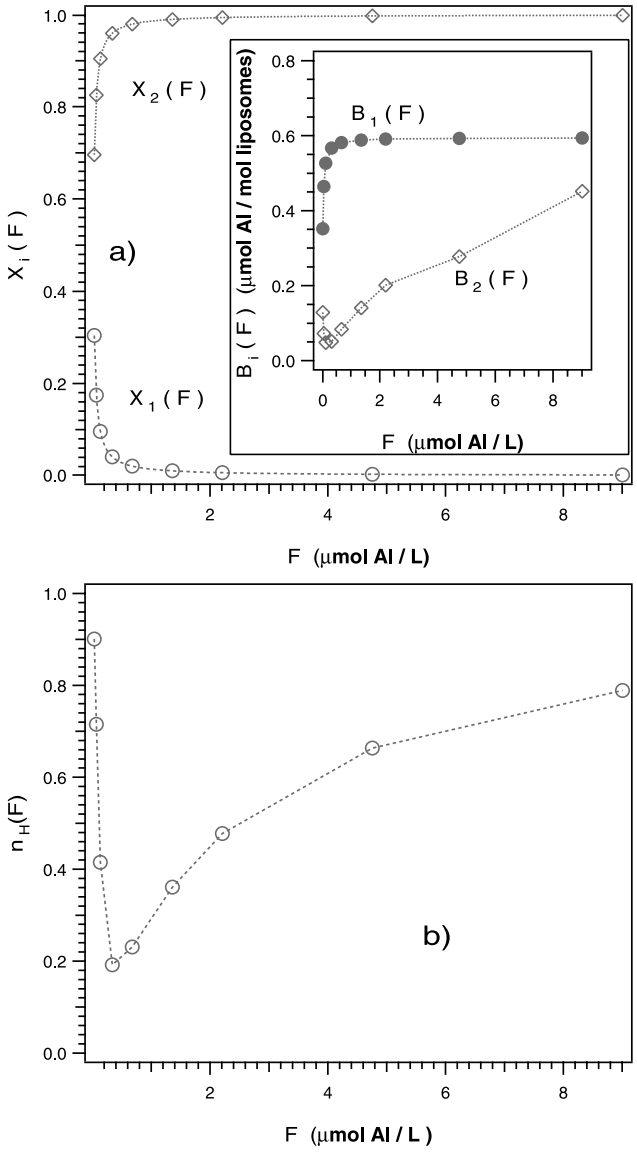

Fig. 19. Al(III)–DPPC liposomes binding process. Dependence on the free Al(III) species concentrations of the molar fractions $x_i(F)$ (a), and $n_H(F)$ (b).

number of binding sites. In the Al-receptor cases reported here the sites are mono-coordinated. Indeed, the binding data fit very well with Eqs. (35), (38) and (45) modified for two sites with mono-coordination; (2) the molar fraction ratio $x_i(F)$ and the consequent evolution of filling the sites. As demonstrated by the analyses depicted in Fig. 16(a) and Fig. 19(a) in both investigated systems, S_1 sites are filled at comparatively lower concentrations of Al than S_2 sites; (3) β_1 values. These parameters indicate the possible effect induced on Al binding to S_1 sites by Al binding to S_2 sites. Theoretically β_1 values are expected between 0 and infinite. Very high values, as those reported here (ca. 214 and 69 (µmol Al/L)$^{-1}$ for trypsin and DPPC liposomes systems, respectively) indicate that the binding of S_2 sites strongly influences the binding to S_1 sites. These results are supported by the Hill factor which for the two investigated systems exhibit values lower than unity. This latter evidence suggests that negative cooperative effects are present in the binding processes investigated. Finally, the standard free energy gaps of the two investigated binding processes were determined. In detail, these energies are ca. 4 and 9 kJ mol^{-1} for Al(III)–trypsin and Al(III)–DPPC liposomes systems, respectively. The interaction energy that characterizes the ligand–receptor linkage commonly is of the order of 0–±10 kJ mol^{-1}.

Liposomes are widely used as a model that mimicks cellular membranes. The thermodynamic approach described here demonstrated that Al(III) interacts with liposomes in two binding sites with very different dissociation constants. The first one has been calculated to be 0.0168 µmol l^{-1} and the second 2.833 µmol l^{-1}. The first is referred to the preferential interaction of Al^{3+} with the polar head of the phospholipid [72], while the second most likely concerns the interaction of Al^{3+} with other peripheral sites consequent to the first interaction. This could contribute to the modification of the membrane structure of the liposomes and thus may make the liposomes more accessible for interaction with Al^{3+}.

In a previous paper we proposed that Al(III) can inhibit the proteolytic activity of trypsin by interacting with the active site of the enzyme [29]. Now, from the study herein reported, we know that the situation is more complicated than that. In fact Al^{3+} interacts with trypsin in two binding sites: the first one ($K_{1,1} = 0.2531$ µmol l^{-1}) most likely concerns its interaction with the active site as we proposed in a previous publication [29]. The second binding site ($K_{2,1} = 1.424$ µmol l^{-1}) concerns, similar to that observed for liposomes, a secondary or peripheral binding site consequent to the α-helix to β-sheet modification of trypsin produced by Al^{3+} as demonstrated by Di Noto et al. [30]. In conclusion the thermodynamic model described here not only confirms what we proposed in previous publications regarding the interaction between liposomes and trypsin with Al(III), but also provides quantitative data for such interactions.

In spite of a large body of evidence on the neurotoxic role of Al(III), the molecular mechanisms that could fully explain such toxicity are far from understood. As a matter of fact, researchers are now dealing with an enormous amount of biological, Al(III)-related data on the basis of bioinorganic molecular information. In our opinion Al(III) chemistry is still in its infancy due to the complexity of the interaction between the metal ion with biological molecules, and the relevant necessity to better understand the role of the metal speciation through the biological targets.

Recently, much attention has been devoted to protease functions in relation, for instance, to amyloid

formation in AD. It has been suggested that proteases, like trypsin, could have a fundamental role in the pathogenesis of such a destructive disease. In addition, Al(III) is considered a potential etiopatogenic factor in AD as well as in other neurodegenerative diseases. We have thus used trypsin, as a paradigmatic model to better understand the role of Al(III) as a remarkable inhibitor of the enzymatic activity as proposed in a previous paper from our laboratory [29]. From the present study we have proved that Al(III) interacts with trypsin in two binding regions. This information seems to indicate that even at relatively low concentration Al(III) could have a relevant role as an enzymatic inhibitor and such an effect is a concentration-dependent phenomenon.

The interaction of Al(III) with the cellular membrane is a crucial point for aluminium toxicology [73]. Al(III) has been demonstrated to interact with biological membranes altering their biophysical structure, and consequently their biological properties [74]. DPPC-liposomes, as utilized in our study, represent a well known biological model for mimicking the interaction between Al(III) and the external cellular membrane. We have also observed Al(III) that appears to have two binding sites with liposomes with affinities differing by two orders of magnitude. The binding on one site remarkably facilitates the interaction of the metal ion with the other binding site through a highly cooperative phenomenon ($\beta_1 = 69.35$ (5) $(\mu mol\ Al/L)^{-1}$), lower with respect than that observed for trypsin.

The thermodynamic model described herein provides, not only qualitative and quantitative information on the interaction of Al(III) with biological targets in two rather different models, as a general methodological approach, but is also a good new way to better project more detailed studies on such interactions using relevant preliminary molecular data.

References

[1] K.A. Connors, Binding Constants, John Wiley and Sons, New York, 1987.
[2] M. Luhmer, K. Bartik, A. Dejaegere, P. Bovy, J. Reisse, Bull. Soc. Chim. Fr. 131 (1994) 603.
[3] A.V. Hill, J. Physiol. 40 (1910) 190.
[4] M. Levitt, M.F. Perutz, J. Mol. Biol. 201 (1988) 751.
[5] G.N. Schrauzer, G.W. Kiefer, K. Tano, P.A. Doemeny, J. Am. Chem. Soc. 96 (1974) 641.
[6] J.C. Ma, D.A. Dougherty, Chem. Rev. 97 (5) (1997) 1303.
[7] T.M. Lohman, M.E. Ferrari, Annu. Rev. Biochem. 63 (1994) 527.
[8] Y. Fraenkel, D.E. Shalev, J.M. Gershoni, G. Navon, Crit. Rev. Biochem. Mol. 31 (4) (1996) 273.
[9] M.S. Wold, Annu. Rev. Biochem. 66 (1997) 61.
[10] A.A. Travers, Annu. Rev. Biochem. 58 (1989) 427.
[11] M.J. Murray, C.P. Flessel, Biochim. Biophys. Acta 425 (1976) 256.
[12] M.N. Williams, D.M. Crothers, Biochemistry 14 (1975) 1944.
[13] B.R. Peterson, T. Mordasini-Denti, F. Diederich, Chem. Biol. 2 (1995) 139.
[14] P. Wallimann, Helv. Chim. Acta 79 (1996) 779.
[15] B. Dietrich, M.W. Hosseini, J.M. Lehn, R.B. Sessions, J. Am. Chem. Soc. 103 (1981) 1282.
[16] B. Linton, A.D. Hamilton, Chem Rev. 97 (5) (1997) 1669.
[17] J. Porath, J. Carlsson, I. Olsson, C. Belfrage, Nature 258 (1975) 598.
[18] M. Castagnola, L. Cassiano, A. Lupi, I. Messana, M. Patamia, R. Rabino, D.V. Rossetti, B. Giardina, J. Chromatogr. Sect. A 694 (1995) 463.
[19] S.J. Kim, T. Takizawa, Makromol. Chem. 176 (1975) 1217.
[20] Y. Markus, G. Howery-Darryl, Ion Exchange Equilibrium Constants, vol. 10, Elsevier Science, New York, 1976.
[21] J.E. Katon, Organic Semiconducting Polymers, Marcel Dekker, New York, 1968.
[22] M. Kaneko, E. Tsuchida, Macromol. Rev. 16 (1981) 397.
[23] V. Di Noto, L. Dalla Via, A. Toninello, M. Vidali, Macromol. Theor. Simul. 5 (1996) 165.
[24] M. Nicolini, P. Zatta, B. Corain (Eds.),Aluminum in Chemistry, Biology and Medicine, Raven Press, New York, 1992, pp. 1–117.
[25] A.C. Alfrey, in: M. Nicolini, P. Zatta, B. Corain (Eds.), Aluminum in Chemistry, Biology and Medicine, Raven Press, New York, 1992, pp. 73–84.
[26] P. Ponte, P. Gonzale-De Whitt, J. Schilling, J. Miller, D. Hsu, B. Greenberg, K. Davis, W. Wallace, I. Lieberburg, F. Fuller, B. Cordell, Nature 331 (1988) 525.
[27] N. Kitaguchi, Y. Takahashi, Y. Tokushima, S. Shiojiri, H. Ito, Nature 311 (1988) 530.
[28] (a) C.R. Abraham, D.J. Selkoe, H. Potter, Cell 52 (1988) 487; (b) D. Selkoe, Neurobiol. Aging 10 (1989) 387.
[29] P. Zatta, C. Bordin, M. Favarato, Arch. Biochem. Biophys. 303 (1993) 407.
[30] V. Di Noto, L. Dalla Via, P. Zatta, J. Raman Spectrosc. 30 (1999) 2099.
[31] P. Zatta, M. Nicolini, Aluminum Toxicity in Infants' Health and Disease, World Scientific, Singapore, 1997, pp. 1–245.
[32] P. Zatta, Acta Med. Romana 35 (1997) 592.
[33] P. Zambenedetti, F. Tisato, B. Corain, P. Zatta, Biometals 7 (1994) 244.
[34] L. Cavallini, V. Di Noto, L. Dalla Via, A. Toninello, M. Vidali, Magn. Res. Biol. Med. 1 (1993) 73.
[35] C.R. Cantor, P.R. Schimmel, Biophysical Chemistry, Part III, Freeman, San Francisco, 1980.
[36] V.L. Hess, A. Szabo, J. Chem. Educ. 56 (1979) 289.
[37] L. Stryer, Biochimica, III ed., Zanichelli, Bologna, 1989.
[38] G. Scatchard, Ann. N.Y. Acad. Sci 51 (1949) 660.
[39] G.S. Eadie, J. Biol. Chem. 146 (1942) 85.
[40] J.D. McGhee, P.H. von Hippel, J. Mol. Biol. 86 (1974) 469.
[41] D.A. Deranleau, J. Am. Chem. Soc. 91 (1969) 4044.
[42] D.A. Deranleau, J. Chem. Phys. 40 (1964) 2134.
[43] I.M. Klotz, D.L. Hunston, Arch. Biochem. Biophys. 193 (1979) 314.
[44] A.V. Hill, Biochem. J. 7 (1913) 471.
[45] F.J.C. Rossotti, H.S. Rossotti, The Determination of Stability Constants, McGraw Hill, New York, 1961.
[46] C. Tanford, Physical Chemistry of Macromolecules, Wiley, New York, 1961.
[47] J. Steinhardt, J.A. Reynolds, Multiple Equilibria in Proteins, Academic, New York, 1969.
[48] G.S. Adair, J. Biol. Chem. 63 (1925) 529.
[49] I.M. Klotz, Acc. Chem. Res. 7 (1974) 162.
[50] I.M. Klotz, Science 217 (1982) 1247.
[51] J.G. Nørby, P. Ottolenghi, J. Jensen, Anal. Biochem. 102 (1980) 318.
[52] P.R. Schimmel, J. Polym Sci. Symp. 54 (1976) 387.
[53] D.M. Crothers, Biopolymers 6 (1968) 575.

[54] G. Schwartz, Eur. J. Biochem. 12 (1970) 442.
[55] S. Le Mée, A. Pierré, J. Markovits, G. Atassi, A. Jacquemin Sablon, J.M. Saucier, Mol. Pharmacol. 53 (1998) 213.
[56] A.N. Lane, T.C. Jenkins, Q. Rev. Biophys. 33 (2000) 255.
[57] E. Renault, M.P. Fontaine-Aupart, F. Tfibel, M. Gardes-Albert, E. Bisagni, J. Photochem. Photobiol. B: Biol. 40 (1997) 218.
[58] H. Klungland, O. Andersen, G. Kisen, P. Alestrom, L. Tora, Mol. Cell. Endocrinol. 95 (1993) 147.
[59] T.M. Lohman, Biopolymers 22 (1983) 1697.
[60] K. Docherty, Gene Transcription: DNA Binding Proteins—Essential Techniques, vol. 2, John Wiley and Sons Inc, New York, 1997.
[61] W. Bujalowski, T.M. Lohman, C.F. Anderson, Biopolymers 28 (1989) 1637.
[62] H.J. Kreuzer, Nonequilibrium Thermodynamics and its Statistical Foundations, Clarendon Press, Oxford, 1981.
[63] V. Di Noto, L. Dalla Via, A. Toninello, Ital. J. Biochem. 46 (1997) 87.
[64] L.D. Byers, J. Chem. Educ. 54 (1977) 352.
[65] L. Dalla Via, V. Di Noto, D. Siliprandi, A. Toninello, Biochim. Biophys. Acta 1284 (1996) 247.
[66] L. Dalla Via, V. Di Noto, A. Toninello, FEBS Lett. 422 (1998) 36.
[67] L. Dalla Via, V. Di Noto, A. Toninello, Arch. Biochem. Biophys. 265 (1999) 231.
[68] L. Dalla Via, V. Di Noto, A. Toninello, Biochem. Pharmacol. 58 (1999) 1899.
[69] M. Favarato, P. Zatta, Toxiol. Lett. 66 (1993) 133.
[70] P. Zatta, D. Cervellin, G. Mattiello, M. Gerotto, F. Lazzari, G. Gasparoni, L. Gomirato, G. Mazzolini, G. Scarpa, V. Zanoboni, G. Pilone, M. Favarato, Trace Elem. Med. 10 (1993) 85.
[71] F. James, M. Roos, Comp. Phys. Commun. 10 (1975) 343.
[72] T. Kiss, P. Zatta, B. Corain, Coord. Chem. Rev. 149 (1996) 329.
[73] P. Zatta, M. Suwalsky, Aluminium, membranes and Alzheimer's disease, in: C. Exley (Ed.), Aluminium and Alzheimer's disease. The Science that Describes the Link, Elsevier, Holland, 2001, p. 279.
[74] M. Suwalsky, B. Ungerer, F. Villena, B. Norris, H. Cardenas, P. Zatta, Brain Res. Bull. 10 (2001) 205.